Monthly Notices
of the
ROYAL ASTRONOMICAL SOCIETY

Mon. Not. R. Astron. Soc. **424,** 2486–2503 (2012) doi:10.1111/j.1365-2966.2012.21175.x

Optical and near-infrared survey of the stellar contents associated with the star-forming complex Sh2-252

Jessy Jose,[1,2⋆] A. K. Pandey,[1] K. Ogura,[3] M. R. Samal,[1,4] D. K. Ojha,[5] B. C. Bhatt,[6] N. Chauhan,[1,7] C. Eswaraiah,[1] H. Mito,[8] N. Kobayashi[8] and R. K. Yadav[1]

[1]*Aryabhatta Research Institute of observational sciencES (ARIES), Manora Peak, Naini Tal 263129, India*
[2]*Indian Institute of Astrophysics, Koramangala, Bangalore 560034, India*
[3]*Kokugakuin University, Higashi, Shibuya-ku, Tokyo 150-8440, Japan*
[4]*Laboratoire d'Astrophysique de Marseille – LAM, Université d'Aix-Marseille & CNRS, UMR7326, 13388 Marseille Cedex 13, France*
[5]*Tata Institute of Fundamental Research, Mumbai 400005, India*
[6]*CREST, Indian Institute of Astrophysics, Koramangala, Bangalore 560034, India*
[7]*Institute of Astronomy, National Central University, Chung-Li 32054, Taiwan*
[8]*Kiso Observatory, School of Science, University of Tokyo, Mitake, Kiso-machi, Kiso-gun, Nagano-ken 397-0101, Japan*

Accepted 2012 April 25. Received 2012 April 16; in original form 2012 February 11

ABSTRACT

We present the analyses of the stellar contents associated with the extended H II region Sh2-252 using deep optical *UBVRI* photometry, slit and slitless spectroscopy along with the near-infrared (NIR) data from Two-Micron All-Sky Survey (2MASS) for an area $\sim 1 \times 1$ deg^2. We have studied the sub-regions of Sh2-252, which includes four compact-H II (CH II) regions, namely A, B, C and E, and two clusters, NGC 2175s and Teutsch 136 (Teu 136). Of the 15 spectroscopically observed bright stars, eight have been identified as massive members of spectral class earlier than B3. From the spectrophotometric analyses, we derived the average distance of the region as 2.4 ± 0.2 kpc, and the reddening $E(B-V)$ of the massive members is found to vary between 0.35 and 2.1 mag. We found that NGC 2175s and Teu 136, located towards the eastern edge of the complex, are the sub-clusters of Sh2-252. The stellar surface density distribution in K band shows clustering associated with the regions A, C, E, NGC 2175s and Teu 136. We have also identified the candidate ionizing sources of the CH II regions. 61 Hα emission sources are identified using slitless spectroscopy. The distribution of the Hα emission sources and candidate young stellar objects (YSOs) with IR excess on the $V/(V-I)$ colour–magnitude diagram (CMD) shows that a majority of them have approximate ages between 0.1 and 5 Myr and masses in the range of 0.3–2.5 $M_\odot$. The optical CMDs of the candidate pre-main-sequence (PMS) sources in the individual regions also show an age spread of 0.1–5 Myr for each of them. We calculated the K-band luminosity functions (KLFs) for the sub-regions A, C, E, NGC 2175s and Teu 136. Within errors, the KLFs for all the sub-regions are found to be similar and comparable to that of young clusters of age <5 Myr. We also estimated the mass function of the PMS sample of the individual regions in the mass range of 0.3–2.5 $M_\odot$. In general, the slopes of the MFs of all the sub-regions are found comparable to the Salpeter value.

Key words: stars: formation – stars: luminosity function, mass function – stars: pre-main-sequence – H II regions – ISM: individual objects: Sh2-252.

1 INTRODUCTION

It is known that most of the stars in the Galaxy are formed in clusters or in OB associations where massive members of the region significantly affect their environment. This is possible in the form of strong stellar winds, intense UV radiation and eventually supernova explosions. These processes can ultimately cause their natal molecular cloud to be destroyed, which, in turn, will put an end to further star formation. However, it has also been observed that the above processes can trigger the birth of new generations of stars (e.g. Elmegreen & Lada 1977) and is likely to influence the key properties

⋆E-mail: jessy@iiap.res.in

of the star formation process such as the initial mass function (IMF), star formation efficiency and the evolution of protostellar discs around the young stars (e.g. Clarke 2007). Keeping in mind the above points, it is important to study the large-scale properties of OB associations so that we can have better understanding of the various processes governing the star formation.

As a continuation of our multi-wavelength analyses of star-forming regions (SFRs; e.g. Jose et al. 2008, 2011; Pandey et al. 2008), an optically bright H II region Sh2-252 (Sharpless 1959; $\alpha_{2000} = 06^{h}09^{m}39^{s}$; $\delta_{2000} = +20^{\circ}29'12''$; $l = 190.04$; $b = +0.48$) has been studied in this paper. It is located in the galactic anticentre direction and is a part of the Gemini OB1 association. Radio and CO surveys have already been done for this region by many authors (e.g. Felli, Habing & Israël 1977; Lada & Wooden 1979; Kömpe et al. 1989; Szymczak, Hrynek & Kus 2000). However, the stellar contents of this region were poorly studied in optical and infrared wavebands. Also, authors have raised arguments regarding the presence of many ionizing sources in this complex (see Felli et al. 1977; Lada & Wooden 1979). However, the massive members of this region have not yet been characterized spectroscopically except three bright sources. In this paper, we use the deep optical data in *UBVRI* bands, slit and slitless spectroscopic observations along with the *JHK* data from Two-Micron All-Sky Survey (2MASS) to identify and classify the massive members, to determine the reddening, distance of the region as well as the age and mass of candidate pre-main-sequence (PMS) sources, and finally to obtain the *K*-band luminosity function (KLF) and IMF. After a brief description of the previous studies on Sh2-252, Section 2 describes various data sets used for the present study. Analyses and results including fundamental parameters of Sh2-252, identification and classification of massive stars in the associated clusters, its various properties such as age, distance, reddening, KLF and IMF are discussed in Section 3, and Section 4 summarizes the results.

1.1 Overview of previous studies on Sh2-252

The low density ($n_e = 9\,\mathrm{cm}^{-3}$) and the relatively large size ($D \sim 20$ pc) of the extended region place Sh2-252 in the class of evolved H II regions (Churchwell 1974). The main source of ionization of Sh2-252 is the central star HD 42088 with a spectral-type O6.5V (Conti & Alschular 1971; Walborn 1972), which is a member of the Gemini OB1 association. In Fig. 1, the Digital Sky Survey-2 (DSS2)-*R* band image of the region around Sh2-252 for an area of $\sim 1.3 \times 1.3$ deg^2 is given, which shows a bright nebula having a diameter of $\sim$30 arcmin with a bright rim (Felli et al. 1977) at the west. See the colour composite image given in Fig. 2 for a close up view. Two stellar clusters were identified in this region optically: one is the dispersed cluster (namely NGC 2175) centred on the nebulosity and the other of smaller diameter (namely NGC 2175s) is located at the north-east of the nebula. Pismis (1970) estimated the distances to these clusters as 1900 and 3500 pc, respectively, and hence NGC 2175s was thought to be a background object. Subsequently, using eight colour photometry, Chavarría, de Lara & Hasse (1987) found that these two clusters are located at a distance of 2.0 kpc and hence claimed that both are associated with Sh2-252. A new near-infrared (NIR) cluster Teutsch 136 (hereafter Teu 136; see Fig. 1) has been identified towards the east of NGC 2175s by Koposov, Glushkova & Zolotukhin (2008). However, they did not make any parameter determination for this cluster. Hence, the association of this object with Sh2-252 needs to be checked. In the literature, the distance to Sh2-252 from spectrophotometric and

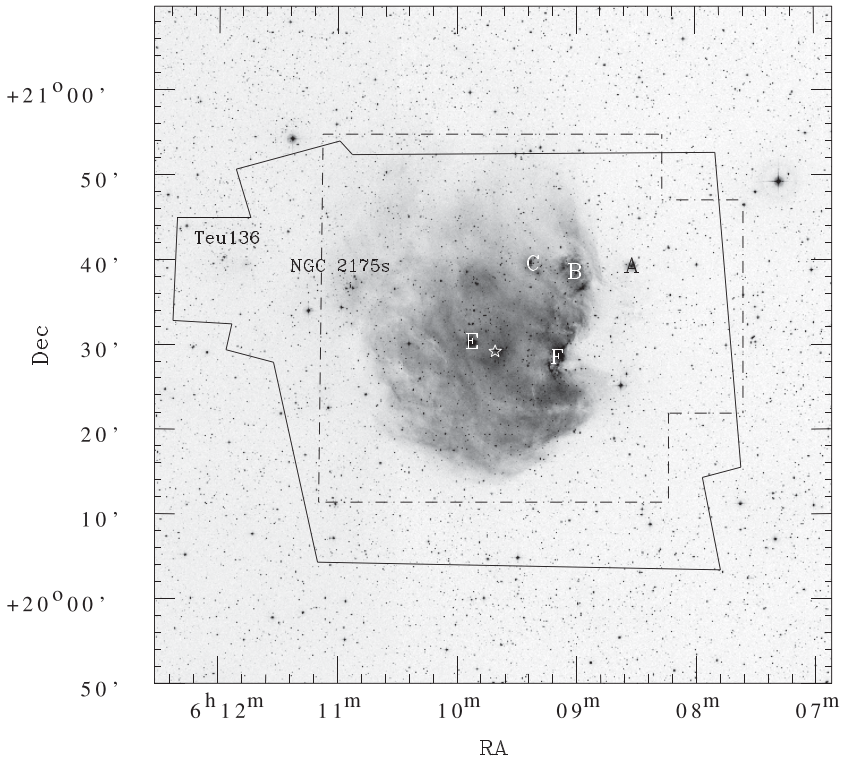

Figure 1. The DSS2-*R*-band image of the region around Sh2-252 for an area of $\sim 1.3 \times 1.3$ deg^2. The locations of the thermal radio sources of the regions A, B, C, E and F identified by Felli et al. (1977) along with the small clusters NGC 2175s and Teu 136 are marked in the figure. The ionizing source (HD 42088) of the H II region is marked using a star symbol. The area covered for the deep optical observations in *V* and *I* bands is shown using continuous lines (polygon), and the thick dot–dashed box represents the area covered with the Hα slitless spectroscopy survey. The abscissa and the ordinates are for the J2000 epoch.

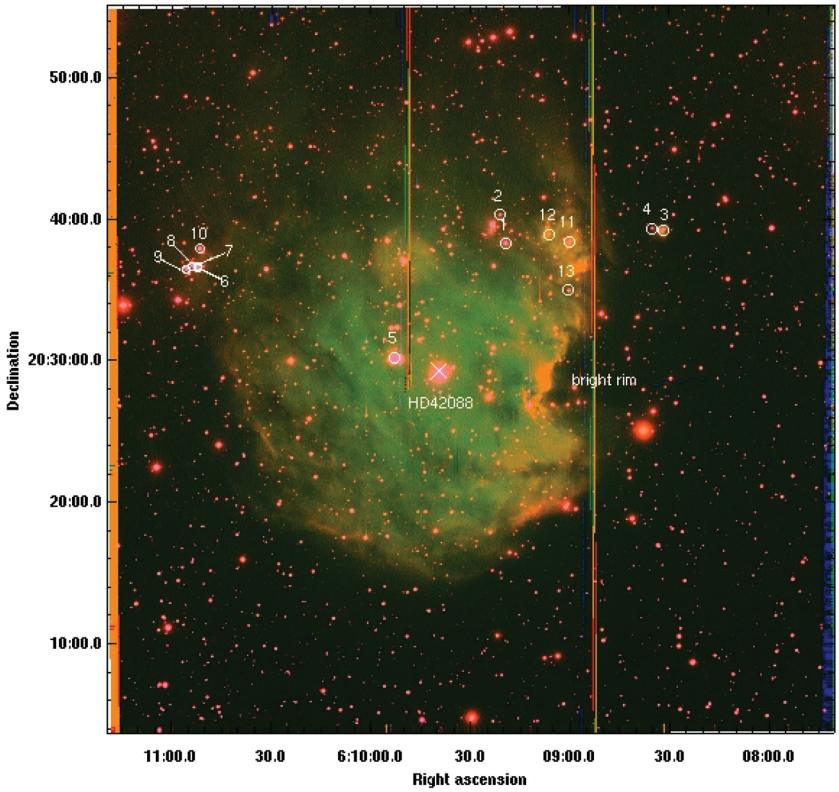

Figure 2. A close-up colour composite view of Sh2-252 reproduced by using the V, Hα and [S II] bands (V: blue; Hα: green; [S II] : red) for an area $\sim$50 $\times$ 50 arcmin^2 obtained from the Kiso observations. The sources numbered are further classified by using spectroscopic observations (see Section 3.1) and their identification is also shown in the figure. The locations of the ionizing source HD 42088 and the bright rim are also marked. The lines in the image are artefacts.

kinematic studies varies between 1.4 and 2.6 kpc (e.g. Pismis 1970; Grasdalen & Carrasco 1975; Reid et al. 2009; Bonatto & Bica 2011). Using the 5 GHz aperture synthesis observations, Felli et al. (1977) detected six extended radio sources towards Sh2-252 labelled as Sh2-252 A to F (see fig. 1 in Lada & Wooden 1979). They have identified four of these sources (A, B, C and E) as compact H II (CH II) regions, probably having a local source of ionization in each of them with a spectral-type later than HD 42088 (i.e. O6.5V). The region F coincides with the optical bright rim (see Fig. 1, and see also Fig. 2 for a close up view) and no internal heating source is found within it (Lada & Wooden 1979). The molecular survey by Lada & Wooden (1979) shows that the most intense CO peak is located very close to Sh2-252A with water and methanol maser emissions within its proximity (Lada & Wooden 1979; Kömpe et al. 1989; Szymczak et al. 2000), which indicates the recent star formation activity towards this region. Most of the region around Sh2-252A seems to be optically obscured; however, there is an embedded cluster visible in NIR and recently Tej et al. (2006) have studied this cluster in detail.

2 OBSERVATIONS AND DATA REDUCTIONS

2.1 Optical CCD imaging

The CCD *UBVRI* observations of Sh2-252 were carried out using the 105-cm Schmidt Telescope of the Kiso Observatory, Japan, on 2004 November 4. The 2K $\times$ 2K CCD with each pixel corresponding to 1.5 arcsec covers a field of $\sim$50 $\times$ 50 arcmin^2 in the sky. The log of observations is tabulated in Table 1.

The CCD *UBVRI* photometry of the central region (α_{2000} = 06^{h}09^{m}39^s; δ_{2000} = +20°29$'$12$''$) of Sh2-252 was carried out using the 104-cm Sampurnanand Telescope (ST) of ARIES, Nainital, India, on 2005 December 2. The 2K $\times$ 2K CCD with a plate scale of 0.37 arcsec pixel^{-1} covers a field of $\sim$13 $\times$ 13 arcmin^2 in the sky. To improve the signal-to-noise ratio (S/N), the observations were carried out in a binning mode of 2 $\times$ 2 pixels. The standard field SA 98 from Landolt (1992) was observed on the same night to apply the atmospheric and instrument corrections to the target field. We then performed point spread function photometry with the DAOPHOT package in IRAF, and derived the extinction coefficients and colour coefficients using the observations of standard field SA 98. The central region of Sh2-252 observed with ST was calibrated by applying these coefficients. The calibration uncertainties between the standard and transformed V magnitudes and $U - B$, $B - V$, $V - R$, $V - I$ colours were $\leq$0.03 mag. The selected isolated stars of this central calibrated region were used to calibrate the wide field observations taken with the Kiso Schmidt Telescope.

We further carried out deep observations in V and I bands using ST for 20 overlapping sub-regions of Sh2-252, to cover an area $\sim$1 $\times$ 1 deg^2 around it. The observations were conducted from 2006 October to 2008 December in good photometric conditions and the log of observations is tabulated in Table 1. Each region was exposed for 60 min in V and 30 min in I band. The combined area of these 20 overlapping regions is shown in Fig. 1 by using solid lines. The secondary standards from the Kiso observations were used to calibrate these individual regions. The final catalogue is made from these three sets of observations, where the magnitudes of the bright ($V < 15$ mag) and faint ($V > 15$ mag) objects were taken from Kiso observations and ST observations, respectively.

Table 1. Log of observations.

$\alpha_{(2000)}$ (h:m:s)	$\delta_{(2000)}$ (d:m:s)	Date of observation	Filter and Exp. time (s) × no. of frames
Kiso[a]			
06:09:32	+20:28:10	2004.11.04	*U*: 60 × 2; B: 20 × 2; V: 10 × 2; R: 10 × 2; I: 10 × 2
ST[b]			
06:09:39	+20:29:12	2005.12.02	*U*: 360 × 2; B: 240 × 2; V: 120 × 2; R: 60 × 2; I: 60 × 2
06:10:09	+20:34:57	2006.10.19	*V*: 600 × 6; *I*: 300 × 6
06:09:14	+20:35:60	2006.10.23	*V*: 600 × 6; *I*: 300 × 6
06:10:09	+20:25:28	2006.10.23	*V*: 600 × 6; *I*: 300 × 6
06:09:18	+20:24:52	2006.12.06	*V*: 600 × 6; *I*: 300 × 6
06:08:06	+20:20:20	2007.01.15	*V*: 600 × 6; *I*: 300 × 6
06:08:06	+20:20:20	2007.01.15	*V*: 600 × 6; *I*: 300 × 6
06:10:56	+20:35:29	2007.01.15	*V*: 600 × 6; *I*: 300 × 6
06:09:11	+20:25:22	2007.11.06	*V*: 600 × 6; *I*: 300 × 6
06:10:54	+20:36:18	2007.11.06	*V*: 600 × 6; *I*: 300 × 6
06:08:51	+20:12:36	2008.01.08	*V*: 600 × 6; *I*: 300 × 6
06:11:56	+20:38:28	2008.01.08	*V*: 600 × 6; *I*: 300 × 6
06:10:25	+20:13:46	2008.04.15	*V*: 600 × 6; *I*: 300 × 6
06:11:31	+20:34:35	2008.04.15	*V*: 600 × 6; *I*: 300 × 6
06:08:31	+20:39:24	2008.12.18	*V*: 600 × 6; *I*: 300 × 6
06:09:29	+20:46:24	2008.12.18	*V*: 600 × 6; *I*: 300 × 6
06:10:24	+20:45:31	2008.12.18	*V*: 600 × 6; *I*: 300 × 6
06:09:42	+20:13:32	2008.12.18	*V*: 600 × 6; *I*: 300 × 6
06:11:09	+20:24:36	2008.12.19	*V*: 600 × 6; *I*: 300 × 6
06:08:23	+20:26:44	2008.12.19	*V*: 600 × 6; *I*: 300 × 6
06:11:16	+20:46:54	2008.12.19	*V*: 600 × 6; *I*: 300 × 6
HCT[c]			
06:09:21	+20:40:37	2005.01.07	Gr5/Hα-Br: 450 × 3; Hα-Br: 90 × 2
06:09:21	+20:24:31	2005.01.08	Gr5/Hα-Br: 450 × 3; Hα-Br: 90 × 2
06:09:60	+20:32:38	2005.01.09	Gr5/Hα-Br: 450 × 3; Hα-Br: 90 × 2
06:09:60	+20:40:39	2005.01.09	Gr5/Hα-Br: 450 × 3; Hα-Br: 90 × 2
06:10:37	+20:40:46	2005.01.09	Gr5/Hα-Br: 600 × 3; Hα-Br: 120 × 2
06:10:37	+20:32:55	2005.02.16	Gr5/Hα-Br: 600 × 3; Hα-Br: 120 × 2
06:10:37	+20:24:28	2005.02.16	Gr5/Hα-Br: 600 × 3; Hα-Br: 120 × 2
06:09:23	+20:48:58	2005.02.17	Gr5/Hα-Br: 600 × 3; Hα-Br: 120 × 2
06:09:23	+20:56:58	2005.02.17	Gr5/Hα-Br: 600 × 3; Hα-Br: 120 × 2
06:10:24	+20:15:44	2005.02.17	Gr5/Hα-Br: 600 × 3; Hα-Br: 120 × 2
06:09:23	+20:16:52	2005.02.17	Gr5/Hα-Br: 600 × 3; Hα-Br: 120 × 2
06:10:54	+20:36:23	2006.01.09	Gr5/Hα-Br: 600 × 3; Hα-Br: 150 × 2
06:08:43	+20:40:47	2007.01.25	Gr5/Hα-Br: 600 × 3; Hα-Br: 120 × 2
06:08:43	+20:32:52	2007.01.25	Gr5/Hα-Br: 600 × 3; Hα-Br: 120 × 2
06:08:43	+20:24:53	2007.01.25	Gr5/Hα-Br: 600 × 3; Hα-Br: 120 × 2
06:08:05	+20:32:57	2007.01.25	Gr5/Hα-Br: 450 × 3; Hα-Br: 90 × 2
06:08:05	+20:40:56	2007.01.25	Gr5/Hα-Br: 450 × 3; Hα-Br: 90 × 2
06:08:43	+20:16:58	2007.01.26	Gr5/Hα-Br: 450 × 3; Hα-Br: 90 × 2
06:08:05	+20:25:01	2007.01.26	Gr5/Hα-Br: 450 × 3; Hα-Br: 90 × 2
06:08:05	+20:33:01	2007.01.26	Gr5/Hα-Br: 450 × 3; Hα-Br: 90 × 2
06:09:46	+20:38:44	2009.11.15	Gr5/Hα-Br: 600 × 3; Hα-Br: 90 × 2
06:09:05	+20:38:44	2009.11.15	Gr5/Hα-Br: 600 × 3; Hα-Br: 90 × 2
06:09:46	+20:28:53	2009.11.15	Gr5/Hα-Br: 600 × 3; Hα-Br: 90 × 2
06:08:31	+20+53:16	2009.11.15	Gr5/Hα-Br: 600 × 3; Hα-Br: 90 × 2
06:10:14	+20+52:54	2009.11.15	Gr5/Hα-Br: 600 × 3; Hα-Br: 90 × 2

[a] 105-cm Schmidt Telescope, Kiso, Japan.
[b] 104-cm Sampurnanand Telescope, ARIES, Naini Tal.
[c] 2-m Himalayan *Chandra* Telescope, IAO, Hanle.

To ensure good photometric quality, we selected only those sources having uncertainty <0.2 mag in *V* band to make the final catalogue. Thus, we obtained photometry of 8791 sources detected at least in *V* and *I* bands with a limiting magnitude of $V \sim 23$ mag.

In order to check the photometry accuracy, we compared our photometry with the *UBV* photometries available in the literature by Grasdalen & Carrasco (1975) and Haikala (1994). The mean difference between our photometry and theirs was ≤0.03 mag in $V, B-V$ and $U-B$, which shows that our photometry is in agreement with the previous studies.

2.2 Hα slitless grism spectroscopy

An Hα emission-line survey of Sh2-252 was conducted between 2005 January and 2009 November. The observations were done in the slitless mode with a grism as the dispersing element using the

HFOSC of Himalayan *Chandra* Telescope (HCT) of Indian Astronomical Observatory (IAO), Hanle, India. The central 2K × 2K pixels of the 2K × 4K CCD were used for data acquisition. The CCD with an image scale of 0.296 arcsec pixel^{-1} covers an area of $\sim 10 \times 10$ arcmin^2 in the sky. A combination of Hα broad-band filter (Hα-Br; 6100–6740 Å) and Grism 5 was used. The resolution of Grism 5 is 870. We observed 25 overlapping sub-regions around Sh2-252 and the area covered for these observations is shown in Fig. 1 using a dot–dashed box. Multiple frames were taken to ensure the presence of Hα emitting sources. The log of the observations is given in Table 1. Hα emission-line stars with an enhancement over the continuum at the Hα line were visually identified. We obtained 61 Hα emitting sources within our surveyed area. The detection limit of the Hα survey is about 3 Å in terms of equivalent width, or $V \sim 22$ in terms of magnitude. In Table 2, we have provided the J2000 coordinates, V-band magnitudes and $V - I$ colours for these emission-line sources, if available.

2.3 Slit spectroscopy

Low-resolution optical spectroscopic observations of 15 optically bright sources in Sh2-252 were made using the Himalayan Faint Object Spectograph and Camera (HFOSC) of HCT. These sources are the probable massive members of Sh2-252 and some of them are the candidate ionizing sources of the sub-H II regions (see Section 3.4.1). The locations of these sources are marked in Fig. 2. The observations were taken on 2009 November 16 and 17. The spectra in the wavelength range 3800–6840 Å with a dispersion of 1.45 Å pixel^{-1} were obtained using the low-resolution Grism 7 with a slit of 2 arcsec width and exposure time of 900 s. One-dimensional spectra were extracted from the bias-subtracted and flat-field corrected images by using the optimal extraction method in IRAF. Wavelength calibration of the spectra was done by using an FeAr lamp source. Spectrophotometric standard star (G191B2B) was observed on these two nights to give the flux calibration to the target spectra.

2.4 Near-infrared data from 2MASS

NIR *JHK* data for point sources within a radius of 30 arcmin around Sh2-252 have been obtained from 2MASS point source catalogue (PSC) (Cutri et al. 2003). To improve the photometric accuracy, we used photometric quality flag (ph_qual = AAA) which gives an S/N $\geq$ 10 and a photometric uncertainty < 0.10 mag. This selection criterion ensures best quality detection in terms of photometry and astrometry (cf. Lee et al. 2005). The *JHK* data were transformed from the 2MASS system to the California Institute of Technology (CIT) system by using the relations given by Carpenter (2001).

2.5 Completeness of the data

To study the luminosity function (LF)/mass function (MF), it is necessary to take into account the incompleteness of the data that could occur due to various factors (e.g. crowding of the stars). We used ADDSTAR routine of DAOPHOT to determine the completeness factor (CF). The procedure has been outlined in detail in our earlier works (see e.g. Pandey et al. 2001). Briefly, we randomly added artificial stars to both V and I images taken with ST in such a way that they have similar geometrical locations but differ in I brightness according to the mean $(V - I)$ colour ($\sim$1.5 mag) of the data sample. The luminosity distribution of artificial stars was

Table 2. Photometric data of Hα emission-line sources in Sh2-252.

$\alpha_{(2000)}$ (h:m:s)	$\delta_{(2000)}$ (°: ′: ″)	V	$V_{\rm err}$	$(V-I)$	$(V-I)_{\rm err}$
06:07:48.61	+20:39:16.3	–	–	–	–
06:07:59.15	+20:29:19.3	21.187	0.053	2.970	0.054
06:08:06.25	+20:33:47.0	18.927	0.010	1.487	0.015
06:08:30.31	+20:37:18.7	–	–	–	–
06:08:31.77	+20:31:42.2	19.754	0.040	3.147	0.051
06:08:33.26	+20:40:38.6	18.049	0.028	2.503	0.056
06:08:35.19	+20:30:22.7	–	–	–	–
06:08:46.41	+20:39:00.4	–	–	–	–
06:08:47.70	+20:29:06.0	–	–	–	–
06:08:50.44	+20:36:41.4	22.081	0.078	3.546	0.080
06:08:51.26	+20:35:36.0	19.797	0.053	2.774	0.070
06:08:51.59	+20:35:37.1	18.179	0.007	2.371	0.012
06:08:52.62	+20:37:28.7	18.200	0.008	2.120	0.012
06:08:55.20	+20:39:33.3	16.876	0.007	1.501	0.011
06:08:57.21	+20:38:45.2	19.694	0.014	2.315	0.018
06:09:01.05	+20:43:10.8	19.455	0.012	2.604	0.014
06:09:02.77	+20:36:43.4	14.427	0.004	0.847	0.014
06:09:13.22	+20:38:20.6	20.888	0.029	2.791	0.032
06:09:14.65	+20:41:26.9	–	–	–	–
06:09:21.23	+20:40:22.6	14.112	0.011	1.365	0.016
06:09:21.31	+20:38:10.0	20.339	0.026	2.960	0.030
06:09:22.16	+20:41:58.1	17.371	0.009	1.975	0.026
06:09:22.64	+20:36:10.2	19.579	0.023	2.549	0.033
06:09:23.43	+20:38:02.7	18.914	0.008	2.456	0.014
06:09:24.04	+20:36:44.8	20.415	0.079	3.276	0.094
06:09:25.36	+20:37:11.0	19.665	0.017	2.968	0.019
06:09:25.54	+20:36:36.0	19.817	0.019	2.605	0.021
06:09:26.31	+20:38:09.4	19.902	0.015	2.920	0.019
06:09:26.77	+20:37:12.7	19.628	0.026	2.430	0.042
06:09:27.19	+20:30:32.6	17.900	0.004	1.990	0.008
06:09:27.24	+20:37:51.6	15.865	0.007	1.484	0.011
06:09:28.57	+20:37:34.8	–	–	–	–
06:09:29.56	+20:41:26.7	20.462	0.022	2.532	0.034
06:09:30.50	+20:37:46.4	20.855	0.031	2.834	0.034
06:09:31.39	+20:38:31.8	19.913	0.014	2.279	0.024
06:09:34.27	+20:44:11.6	18.810	0.007	2.805	0.010
06:09:35.25	+20:31:15.3	19.371	0.013	2.075	0.021
06:09:37.71	+20:37:55.8	20.013	0.014	2.731	0.019
06:09:39.30	+20:38:43.6	21.565	0.060	2.546	0.069
06:09:39.38	+20:34:28.9	19.130	0.010	2.231	0.013
06:09:41.35	+20:43:37.7	17.666	0.006	1.729	0.010
06:09:41.77	+20:31:25.0	19.140	0.013	2.421	0.018
06:09:51.52	+20:28:33.1	20.623	0.046	3.078	0.049
06:09:51.67	+20:30:06.6	14.373	0.017	1.066	0.025
06:09:55.35	+20:33:35.0	17.166	0.004	2.254	0.006
06:09:55.44	+20:40:13.7	15.980	0.003	1.613	0.005
06:10:05.45	+20:35:53.7	18.218	0.004	1.902	0.007
06:10:14.97	+20:43:22.5	15.356	0.005	1.340	0.007
06:10:35.48	+20:29:26.3	18.628	0.010	1.795	0.033
06:10:37.84	+20:33:42.4	19.289	0.007	2.267	0.009
06:10:38.58	+20:39:24.9	17.006	0.008	1.614	0.018
06:10:39.95	+20:33:36.4	19.517	0.009	2.196	0.011
06:10:43.60	+20:35:41.1	18.487	0.005	2.320	0.011
06:10:45.36	+20:41:55.3	19.274	0.007	2.494	0.008
06:10:46.37	+20:34:06.0	18.500	0.004	2.290	0.006
06:10:48.22	+20:31:45.7	19.143	0.018	2.250	0.023
06:10:49.02	+20:35:23.9	20.078	0.015	1.912	0.020
06:10:49.94	+20:36:59.0	18.485	0.005	1.968	0.007
06:10:50.96	+20:31:05.8	21.582	0.121	3.213	0.123
06:10:53.67	+20:32:23.6	13.556	0.005	1.104	0.005
06:10:57.60	+20:42:46.3	18.427	0.006	1.866	0.010

Table 3. CFs of optical and 2MASS *K*-band data within the sub-regions Sh2-252C and NGC 2175s.

Mag. range	Optical Sh2-252C	Optical NGC 2175s	2MASS *K* band Sh2-252C	2MASS *K* band NGC 2175s
10–11	1.00	1.00	1.00	1.00
11–12	1.00	1.00	0.99	0.99
12–13	1.00	1.00	0.97	0.97
13–14	1.00	1.00	0.92	0.95
14–15	1.00	1.00	0.85	0.88
15–16	1.00	1.00	0.67	0.70
16–17	1.00	1.00	–	–
17–18	0.99	0.99	–	–
18–19	0.96	0.98	–	–
19–20	0.89	0.92	–	–
20–21	0.80	0.85	–	–
21–22	0.59	0.71	–	–

chosen in such a way that more number of stars were inserted towards the fainter magnitude bins. The frames were reduced using the same procedure used for the original frames. The ratio of the number of stars recovered to those added in each magnitude interval gives the CF as a function of magnitude. The minimum value of the CF of the pair (i.e. *V* and *I* bands) was used to correct the data incompleteness. It is to be noted that the spatially varying nebular background (see. Fig. 2) and stellar crowding characteristics (see Fig. 9) could affect the local completeness limit. In order to account for this, we estimated the CFs of two representative sub-regions Sh2-252C and NGC 2175s, and the values obtained are given in Table 3. The CFs of both the regions seem to be agreeing well with each other except for the faint magnitude bin, where the variation seems to be significant.

We also estimated the CFs of the 2MASS data using the *K*-band images from the archive around the regions Sh2-252C and NGC 2175s. Using the DAOPHOT/ALLSTAR package, we detected all the stars in the 2MASS PSC, with photometry accuracy better than 0.05 mag. We then performed the completeness analysis using ADDSTAR routine as mentioned above. The CFs thus obtained for the two sub-regions are given in Table 3. The CFs of both the regions seem to be more or less similar in all the magnitude bins.

3 RESULTS

3.1 Spectral classification of the optically bright sources in Sh2-252

The targets for the low-resolution spectroscopy were selected on the basis of their brightness, their location within 2 arcmin radius of the sub-regions of Sh2-252 (see Fig. 2) and their location on the optical colour–magnitude diagram (CMD; Fig. 7). The coordinates of these sources are given in Table 4. To determine the spectral type, we extracted the low-resolution, one-dimensional spectrum of each source. The flux-calibrated, normalized spectrum of these sources is shown in Fig. 3.

In order to classify the stars earlier than B3, we used the criteria given by Walborn & Fitzpatrick (1990). For later-type stars we used the criteria given by Jacoby, Hunter & Christian (1984) and Torres-Dodgen & Weaver (1993). Spectra of O and B stars have the features of hydrogen, helium and other atomic lines (e.g. O II, C III, Si III, Si IV, Mg II). Hydrogen and helium lines are usually seen in absorption for dwarfs whereas they may be in emission in supergiants. In the case of early-type stars, the ratio of He I 4471/He II 4542 is a primary indicator of the spectral type and the ratio is greater than 1 for spectral type later than O7. The line strength of He II gets weaker for late O-type stars and He II 4686 is last seen in B0.5-type stars (Walborn & Fitzpatrick 1990). If the spectrum displays He II line at 4200 Å, along with the O II/C III blend at 4650 Å, it indicates that the spectral type of the star must be earlier than B1. The absence of He II 4200, He II 4686 and Mg II 4481 and the weak features of silicon lines along with the weak O II/C III blends at 4070 and 4650 are the supporting criteria in the B1–B2 range. For type B2, He I is in its maximum and for later types Si II 4128-4130 and Mg II 4481 appear stronger (Walborn & Fitzpatrick 1990). The presence of the He I lines in absorption constrains the spectral types to be earlier than B5–B7. The presence of the spectral lines Mg II 4481 and Si III 4552 is an indication of evolved early B-type stars. The spectral lines such as Na I 5893, He I, Hα, Ca I 6122, 6162, Fe II 6456 are used to classify the late-type sources (Torres-Dodgen & Weaver 1993). Finally, the spectral type was assigned to each source by a visual comparison to the standard library spectra given in the literature (Jacoby et al. 1984) and our classification is given in Table 4. However, because

Table 4. Details of spectroscopically identified stars.

ID	$\alpha_{(2000)}$ (h:m:s)	$\delta_{(2000)}$ (d:m:s)	V (mag)	$B-V$ (mag)	A_V (mag)	Spectral class	V_0-M_V (mag)	D (pc)	Associated with
1	06:09:19.51	+20:38:20.61	11.79	0.32	1.66	B2.5V	12.15	2690	C
2	06:09:21.18	+20:40:23.01	14.11	0.90	–	B9Ve	–	–	C
3	06:08:32.10	+20:39:19.09	13.88	–	6.5	O9.5V	11.63	2120	A
4	06:08:35.31	+20:39:24.49	12.50	0.30	1.28	B8V	11.47	1970	A
5	06:09:52.63	+20:30:16.60	11.10	0.36	1.92	B1V	12.37	2980	E
6	06:10:52.84	+20:36:42.00	11.05	–	1.93	B1.5V	11.94	2440	N2175s
7	06:10:52.83	+20:36:34.00	10.34	–	1.67	B1V	11.87	2370	N2175s
8	06:10:54.10	+20:36:44.77	11.51	0.49	2.27	B2V	11.69	2180	N2175s
9	06:10:55.97	+20:36:29.65	10.92	0.49	2.40	B0.5V	12.12	2660	N2175s
10	06:10:52.02	+20:38:00.50	10.95	0.32	–	F6V	–	–	N2175s
11	06:09:00.14	+20:38:28.14	10.79	0.55	2.62	B0V	12.17	2710	B
12	06:09:06.49	+20:39:01.43	12.60	0.17	0.88	B8V	11.97	2480	B
13	06:09:00.65	+20:35:04.74	12.32	0.74	–	K0V	–	–	B
14	06:11:46.38	+20:39:21.10	13.74	–	2.77	B6V	11.87	2360	Teu 136
15	06:11:45.10	+20:39:20.42	15.85	–	–	K0V-III	–	–	Teu 136
16[a]	06:09:39.60	+20:29:15.43	7.55	0.06	1.14	O6.5V	11.74	2230	–

[a]Data taken from Pismis (1977).

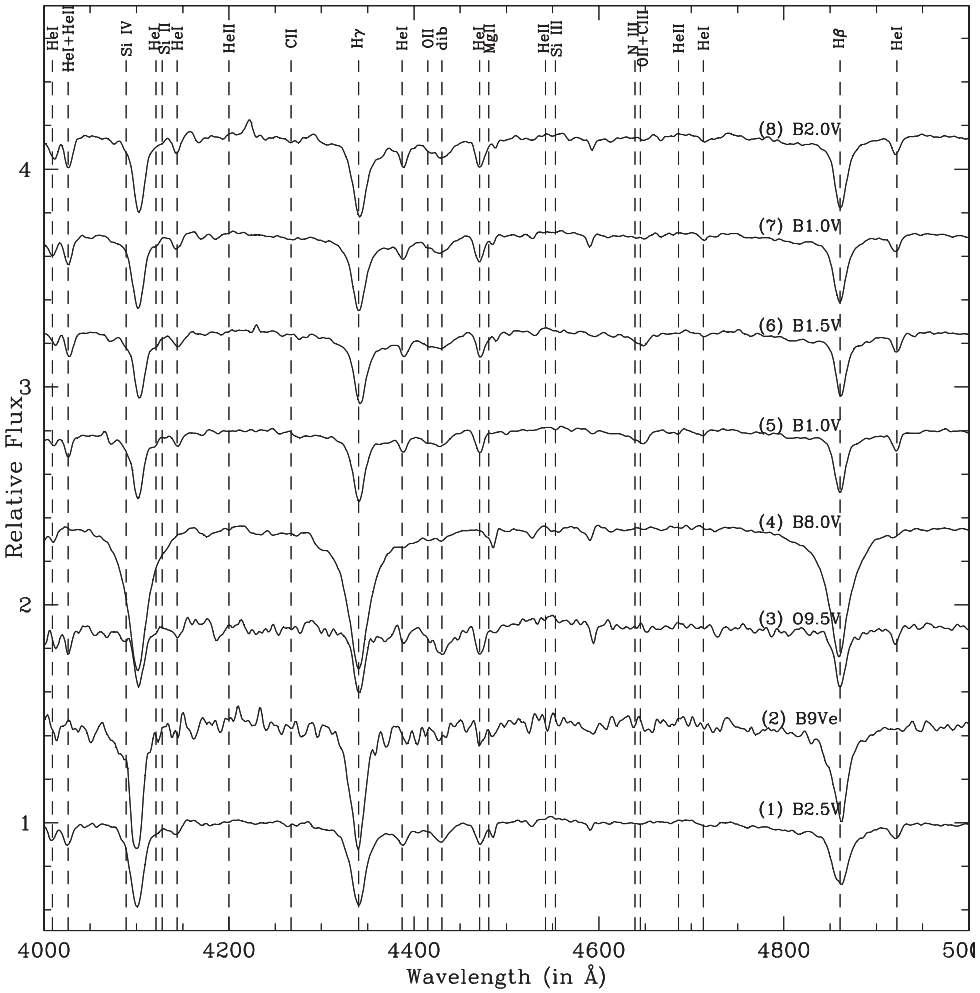

Figure 3. Flux-calibrated normalized spectra for the optically bright sources in Sh2-252. The star IDs and spectral classes identified are given in the figure. Important spectral lines are marked.

of low-resolution observations an uncertainty of ±0.5 to 1 in the sub-class identification is expected.

Eight out of the 15 stars observed are found to have spectral types earlier than B3V. The sub-H II regions of Sh2-252 (i.e. A, B, C and E) are found to have at least one star of spectral type earlier than B3V (i.e. stars 1, 3, 5 and 11). It is quite interesting to note that the remaining four early-type sources (i.e. stars 6, 7, 8 and 9) belong to the small cluster NGC 2175s. The star 2 shows Hα 6563 line in strong emission (not shown in Fig. 3). This star also shows strong NIR excess emission in the $(J - H)/(H - K)$ colour–colour (CC) diagram (see Fig. 5) most likely originating from the extensive, hot circumstellar material around the star. The emission-line spectra as well as the NIR excess emission are the primary indicators of a young stellar object (YSO) and hence we tentatively put this object in the Herbig Be category.

The spectral types of some of these sources have already been mentioned in the literature. On the basis of the 1280 MHz radio continuum flux, Tej et al. (2006) predicted the spectral type of the ionizing source of Sh2-252A as B0-B0.5V. The star 3, located within 2 arcmin of the radio peak of Sh2-252A, is the brightest source in the optical and NIR wavelengths. This could be the ionizing source of Sh2-252A. We classify this source as an O9.5V-type star, which is in agreement with the classification by Tej et al. (2006). The star 5, the probable exciting source of Sh2-252E, had been assigned a spectral type between O8 to B0.5V by Garnier & Lortet-Zuckermann (1971) and B1V by Grasdalen & Carrasco (1975). Our classification (B1V) is in good agreement with that given by Grasdalen & Carrasco (1975). The star 11, the brightest source of Sh2-252B, was classified as B2V by Grasdalen & Carrasco (1975). However, our classification (B0V) leads to a class slightly earlier than their study. The star 2 had been identified as a probable Herbig Be source of spectral type B9 by Chavarría et al. (1989), which seems to match with our classification. Thus present spectral classifications within errors are in accordance with those reported in the literature.

3.2 Reddening, membership and distance of the bright sources in Sh2-252

The extinction in a SFR arises due to two distinct sources: (1) the general interstellar medium in the foreground of the region $[E(B - V)_{\rm min}]$, and (2) the localized cloud associated with the region $[E(B - V)_{\rm local} = E(B - V) - E(B - V)_{\rm min}]$, where $E(B - V)$ is the observed reddening of the star embedded in the local cloud. The presence of the molecular cloud (Lada & Wooden 1979) and the nebulosity associated with Sh2-252 as evident in Fig. 2 would give rise to variable extinction within this region. To estimate the

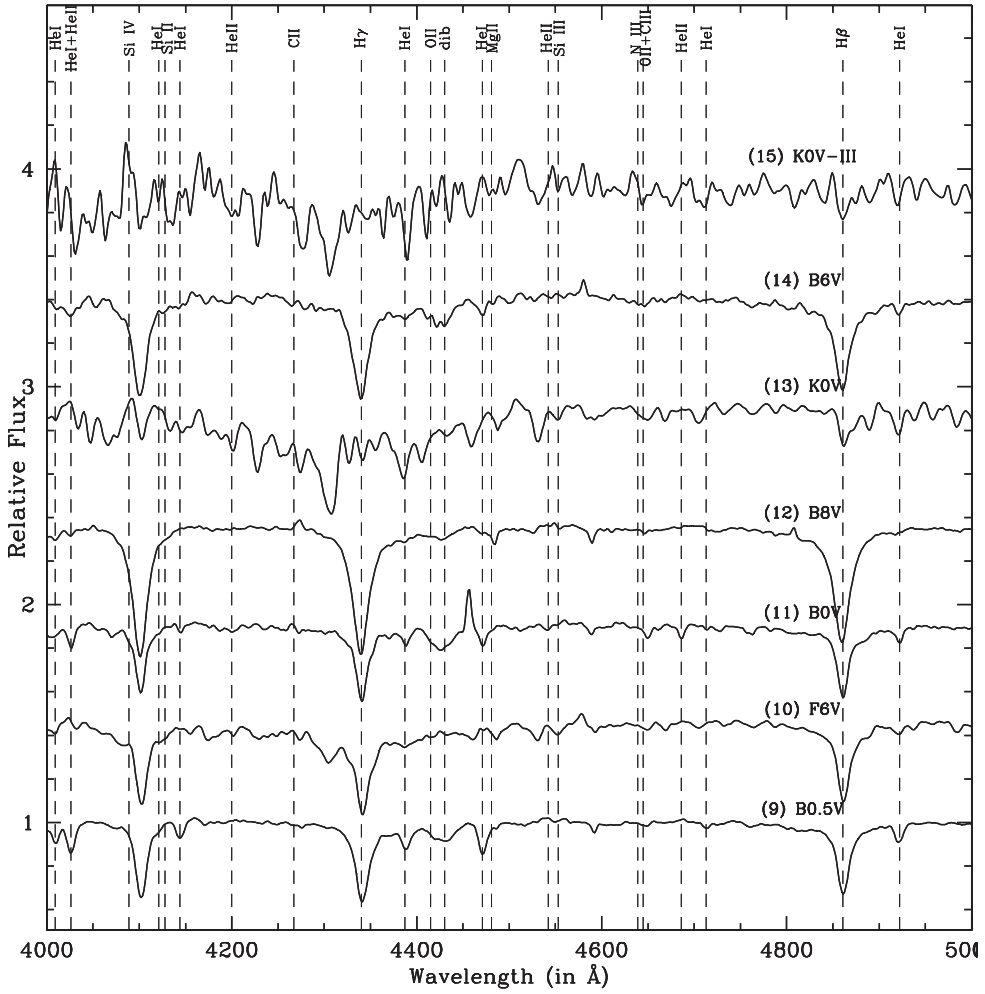

Figure 3 – *continued*

extinction towards the region, we used the $(U-B)/(B-V)$ CC diagram. Fig. 4 shows the $(U-B)/(B-V)$ CC distribution of all the stars detected in our Kiso observations, where the spectroscopically observed sources are numbered in red. It is to be noted that some of the spectroscopically observed stars are not covered/detected in the U and B bands, hence they are not included in Fig. 4. The star 16, which is the ionizing source of Sh2-252 (i.e. HD 42088), was saturated in our observations. Hence the data for this star are taken from Pismis (1977). The zero-age main sequence (ZAMS) by Girardi et al. (2002) that is reddened by $E(B-V)=0.23$ mag along the reddening vector having a normal slope of $E(U-B)/E(B-V)=0.72$ seems to match with the first sequence of distribution in Fig. 4. However, the majority of the spectroscopically identified stars earlier than spectral type B3 show $E(B-V)$ in the range 0.35–0.75 mag. The stars 10, 13 and 15 are found to be late-type stars and hence may not be associated with Sh2-252. Assuming that uncertainties in the $(U-B)$ and $(B-V)$ colours mainly originate from their calibration (Section 2.1), the typical error in the estimation of $E(B-V)$ would be $\sim$0.04 mag. A careful inspection of the CC diagram indicates the presence of further reddened population at $(B-V)$ $\sim$ 0.65–0.90 mag. Some of them may be the reddened members of the Sh2-252 region. The population having $E(B-V)\sim 1.00$–1.25 mag could be part of the background Norma-Cygnus arm as discussed by Carraro et al. (2005) and Pandey, Sharma & Ogura (2006).

We also estimated the individual reddening $E(B-V)$ of spectroscopically classified stars. We used the relation $E(B-V)=(B-V)-(B-V)_0$, where $(B-V)$ is the observed colour and $(B-V)_0$ is the intrinsic colour taken from Schmidt-Kaler (1982). Some of the stars do not have the $(B-V)$ data (i.e. stars 3, 6, 7 and 14) and for these stars A_V was calculated by using the relations $E(J-H)=(J-H)-(J-H)_0$ and $A_V=E(J-H)/0.11$ (Cohen et al. 1981), where $(J-H)$ colours were taken from 2MASS and intrinsic $(J-H)_0$ colours were taken from Koornneef (1983). The A_V thus calculated are given in Table 4. The range of reddening of the spectroscopically identified stars shown in Fig. 4 agree well with that given in Table 4.

In Fig. 5 we have shown the $(J-H)/(H-K)$ CC distribution of all the spectroscopically identified stars in Sh2-252. The sources falling towards the right of the reddening vector are considered to have NIR excess (see Section 3.4.3 for details). The star 2 falls in the location where Herbig Ae/Be stars are generally found (Hernandez et al. 2005) and this justifies our spectral classification of this source as a Herbig Be type (see sect. 3.1). The figure also shows that star 3 is highly reddened when compared to other massive stars in the field.

The estimated spectral classification, apparent magnitudes and extinction of the massive members of Sh2-252 (Table 4) enable us to derive their distances. Using the present spectral classification along with A_V and V values from Table 4 and M_V values from the

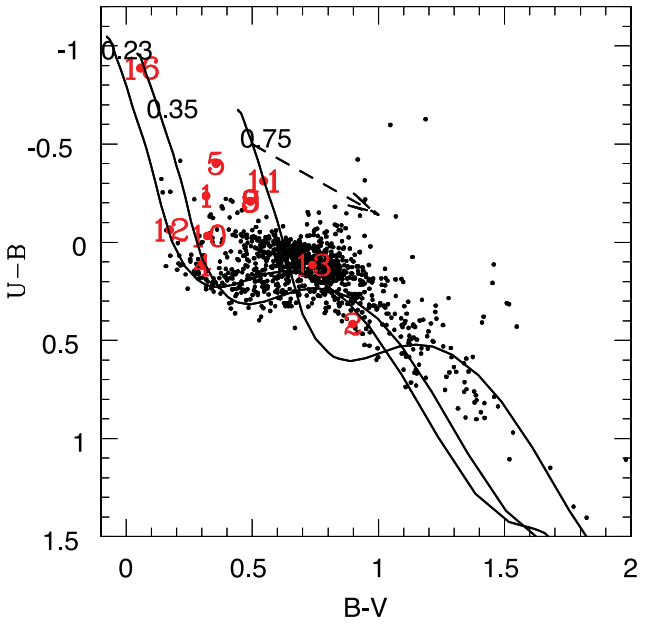

Figure 4. $(U-B)/(B-V)$ CC diagram for the stars in Sh2-252 region. The continuous curves represent the ZAMS by Girardi et al. (2002) shifted along the reddening slope of 0.72 (shown as the dashed line) for $E(B-V)=0.23$, 0.35 and 0.75 mag, respectively. The spectroscopically observed sources are shown in red with their IDs as given in Fig. 2 and in Table 4.

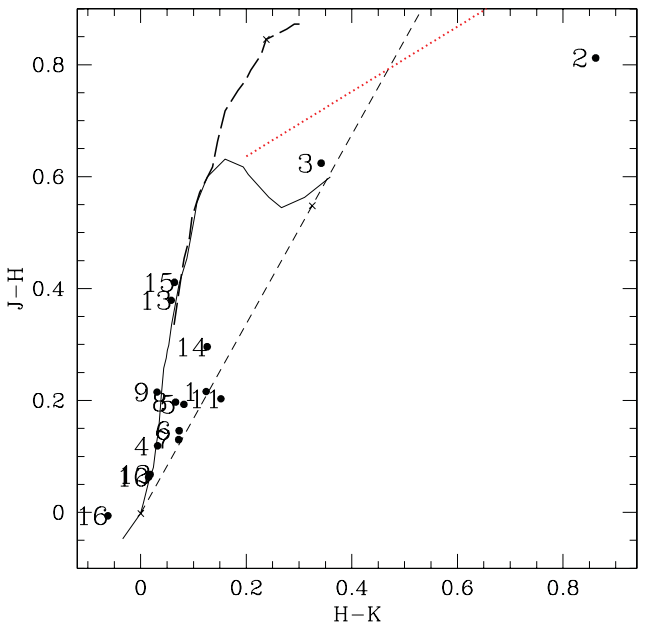

Figure 5. $(J-H)/(H-K)$ CC distribution of the spectroscopically classified stars in Sh2-252. Their IDs are as given in Table 4. The loci for dwarfs (thin solid curve) and giants (thick dashed curve) are from Bessell & Brett (1988). The red dotted lines represent the intrinsic locus of CTTSs (Meyer, Calvet & Hillenbrand 1997). The dashed line in black represents the reddening vector drawn from the early dwarf locus (Cohen et al. 1981).

table of Schmidt-Kaler (1982), we estimated the intrinsic distance modulus $(V_0 - M_V)$ of each source and the same is given in Table 4. The average value of the intrinsic distance modulus is found to be 11.91 ± 0.18 mag, which corresponds to a distance of 2400^{+220}_{-180} pc. We also calculated the intrinsic distance modulus $(K_0 - M_K)$ of

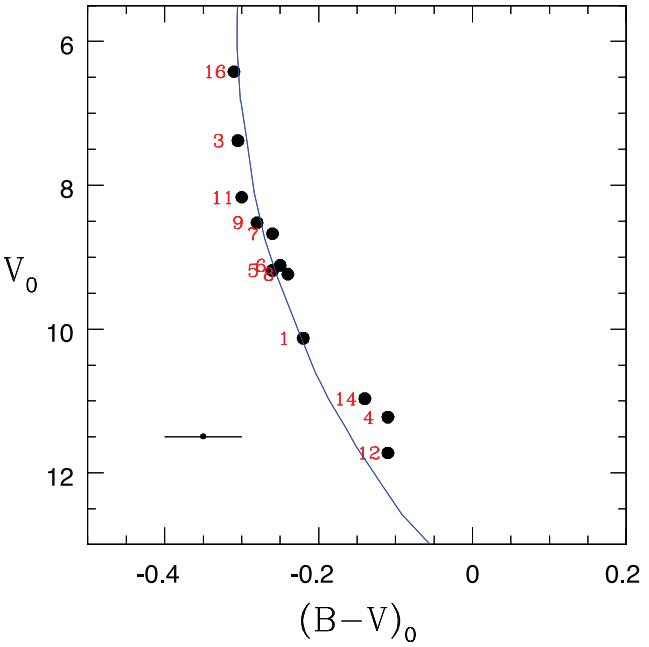

Figure 6. $V_0/(B-V)_0$ CMD for the spectroscopically identified massive member stars in Sh2-252. The continuous curve represents the ZAMS locus by Girardi et al. (2002) corrected for the distance of 2.4 kpc. The sources are numbered as in Table 4. The average error in colour is shown in the lower left-side of the figure.

each source based on the observed colours from 2MASS data and intrinsic colours and absolute magnitudes from Koornneef (1983) and Schmidt-Kaler (1982), respectively. The average value of the intrinsic distance modulus using 2MASS data was found to be 11.80 ± 0.10 mag, which is comparable with that of the intrinsic distance modulus estimated from optical data within errors. Fig. 6 shows dereddened $V_0/(B-V)_0$ CMD for the probable main sequence (MS) members of Sh2-252 identified spectroscopically. In this figure, we have also plotted the theoretical ZAMS locus for solar metallicity ($Z = 0.02$) by Girardi et al. (2002), adjusted for the distance of 2.4 kpc, which seems to be matching well with the distribution of the probable MS members. The present distance estimate is in good agreement with that of Georgelin & Georgelin (1970; 2.4 kpc), Neckel, Klare & Sarcander (1980; 2.3 kpc) and Chavarría et al. (1987; 2.3 kpc). At the same time, it is also in agreement with the distance estimates by Grasdalen & Carrasco (1975; 2.6 kpc) and Reid et al. (2009; 2.1 ± 0.03 kpc) within errors.

An important issue to be discussed here is the association of NGC 2175s and Teu 136 with Sh2-252. NGC 2175s is a small, optically visible cluster located at the east of Sh2-252 (at $\alpha_{2000} = 06^{\rm h}10^{\rm m}52^{\rm s}$; $\delta_{2000} = +20^\circ36'36''$; see Figs 1 and 2). The photoelectric study by Pismis (1970) puts this cluster at a distance of 3500 pc. However, in the present spectroscopic observations, we identified four early B type members of this cluster (i.e. stars 6, 7, 8 and 9; see Table 4), and the distance estimates of these four sources are in good agreement with that of the average distance of Sh2-252. Hence, our spectroscopic analysis supports the association of NGC 2175s with the Sh2-252 complex. Similarly, the cluster Teu 136 was identified as an NIR embedded cluster by Koposov et al. (2008) in a survey of the 2MASS catalogue designed to identify new open clusters. Located at coordinates $\alpha_{2000} = 06^{\rm h}11^{\rm m}56^{\rm s}$; $\delta_{2000} = +20^\circ40'14''$, ~15 arcmin NE of NGC 2175s, this cluster lies close to the eastern edge of the Sh2-252 complex. We obtained spectra of two stars

located close to this cluster (i.e. stars 14 and 15) and the distance of star 14 (see Table 4) seems to match well with that of Sh2-252. Also, the spectral types of two bright stars at the centre of this cluster, which are saturated in our photometric observations, are given as B1.5 and B2.5, respectively, in Reed (2003). The average distance modulus of these two stars comes out to be 11.74 mag, which seems to match with the average distance modulus of the Sh2-252 complex. Therefore, we presume that Teu 136 could be associated with the Sh2-252 complex too. Hence, in this paper we report that the NIR cluster Teu 136 as a sub-cluster of the Sh2-252 complex.

In Fig. 7, we show the $V/(V-I)$ CMD for all the stars detected in our optical photometry. Spectroscopically identified massive MS members are shown with large filled circles in red, where the brightest star is HD 42088. The solid curves are the ZAMS by Girardi et al. (2002) shifted for the distance of 2.4 kpc and reddening $E(B-V) = 0.35$ and $E(B-V) = 0.75$, respectively. The average photometric uncertainty in V magnitudes and $(V-I)$ colours estimated from the difference between the input and recovered magnitudes of the artificial stars (see Section 2.5) are shown in the left-hand side of the figure. The CMD clearly shows a broad MS band down to $V \sim 14$ mag with a significant number of sources located within the reddening strips [i.e. $E(B-V) = 0.35$ to 0.75 mag]. In the absence of spectroscopic information, it is difficult to assign membership for these bright sources. Since Sh2-252 is located close to the Galactic plane ($l = 190.04$; $b = +0.48$) at a distance of 2.4 kpc, it is quite natural that the region could be significantly contaminated by Galactic field MS and giant populations. The extinction variation inside the

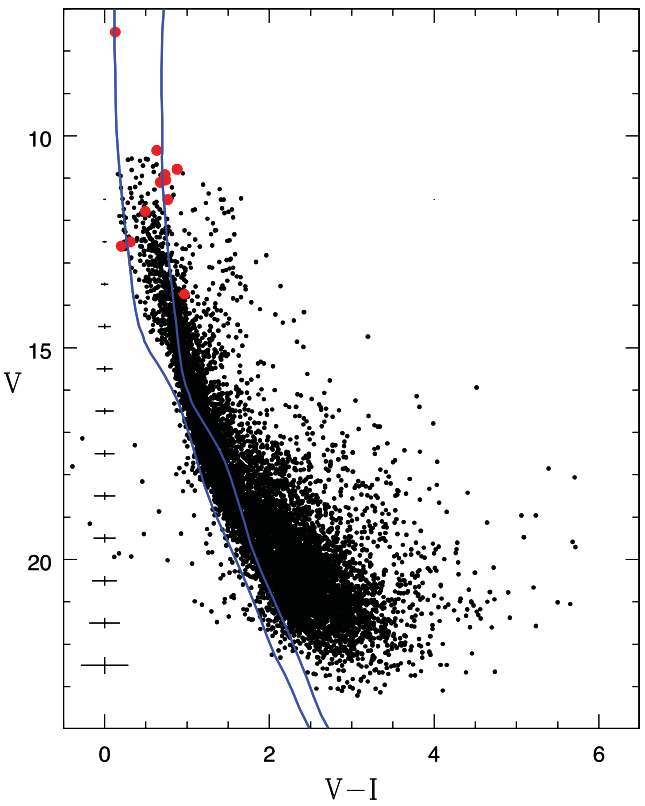

Figure 7. $V/(V-I)$ CMD for all the stars detected in our optical photometry. The solid curves are the ZAMS from Girardi et al. (2002) corrected for the distance 2.4 kpc and reddening $E(B-V) = 0.35$ and $E(B-V) = 0.75$, respectively. The sources marked with red filled circles are the spectroscopically identified MS members of Sh2-252. The average error in $(V-I)$ colour as a function of magnitude is shown in the left-hand side of the figure.

Sh2-252 region may cause a spread in the MS both for the member sources and for the background sources. A significant number of sources can also be noticed towards the right side of the ZAMS, part of which could be PMS stars.

3.3 Age and mass distribution of candidate YSOs in Sh2-252

In the absence of proper motion data, the membership of Sh2-252 can be established by identifying stars with indicators of youth. YSOs emit excess radiation in the infrared in comparison to MS stars due to the thermal emission from their circumstellar material. So YSOs can be identified on the basis of their infrared excess emission. We have also carried out a YSO survey of the Sh2-252 region using the 2MASS and the *Spitzer*-infrared array camera (IRAC) data sets (3.6, 4.5, 5.8 and 8.0 μm) and the detailed analyses will be presented in a forthcoming paper. A total of 96 Class I and 400 Class II YSOs are identified within this complex on the basis of IR colour excess criteria given by Gutermuth et al. (2009). The possible contamination, due to PAH-emitting galaxies, broad-line active galactic nuclei, etc., has been excluded using the criteria given by Gutermuth et al. (2009). Similarly, the presence of Hα emission line is considered as a significant characteristic of a YSO with ongoing disc accretion process (e.g. Dahm 2005). We identified 61 Hα emission-line stars in our slitless spectroscopy survey of the Sh2-252 region (see section 2.2). Our deep photometry provided V and I counterparts for 15 Class I, 179 Class II and 54 Hα emission-line sources. Of these 54 Hα sources, four are Class I and 33 are Class II YSOs. The distribution of these candidate YSOs, i.e. Class I, Class II and Hα emission-line sources on the $V/(V-I)$ CMD, is shown in Fig. 8 by using red squares, green triangles and blue triangles, respectively. The distance to Sh2-252 is adopted as 2.4 kpc as estimated on the basis of the spectroscopic analyses mentioned in Section 3.2. In Fig. 8 the ZAMS (the thick solid curve) by Girardi et al. (2002) and the PMS isochrones (dashed curves) by Siess, Dufour & Forestini (2000) for age 0.1 and 5 Myr are also shown. The ZAMS and isochrones are shifted for the distance of 2.4 kpc and average reddening i.e. $E(B-V) = 0.5$ mag. The average photometric uncertainty in V magnitudes and $(V-I)$ colours estimated from the completeness simulation (see Section 2.5) close to region C are shown in the right-hand side of the figure. The distribution of YSOs on the $V/(V-I)$ CMD is an ideal tool to estimate the approximate ages of YSOs. It is evident from this figure that a majority of the YSOs in Sh2-252 are distributed between the PMS isochrones of age 0.1 and 5 Myr, which shows that the region Sh2-252 significantly comprises young sources. However, the photometric uncertainty, differential reddening, binarity, different evolutionary stages of YSOs, etc. can cause a spread in the CMD. The spectroscopic analysis of the member stars shows that the reddening A_V in the region varies between 0.9 and 6.5 mag (see Table 4). Also, the NIR CC analysis of the candidate PMS sources shows that they are reddened up to 8 mag (see Section 3.4.3), which suggests that the region is significantly affected by the differential reddening. Similarly, the photometric uncertainties in the case of YSOs (see Fig. 8) may be relatively large due to crowding and variable background, which may cause the scatter in the distribution of the Class I and Class II sources in the CMD. Hence the differential reddening and photometric uncertainty would have an impact on the observed age spread in the CMD. The detailed spatial distribution and evolutionary status of the YSOs in the Sh2-252 region will be analysed in a forthcoming paper. In Fig. 8 we have also shown the PMS evolutionary tracks by Siess et al. (2000) (thin solid curves) for various mass bins (the value of mass for each

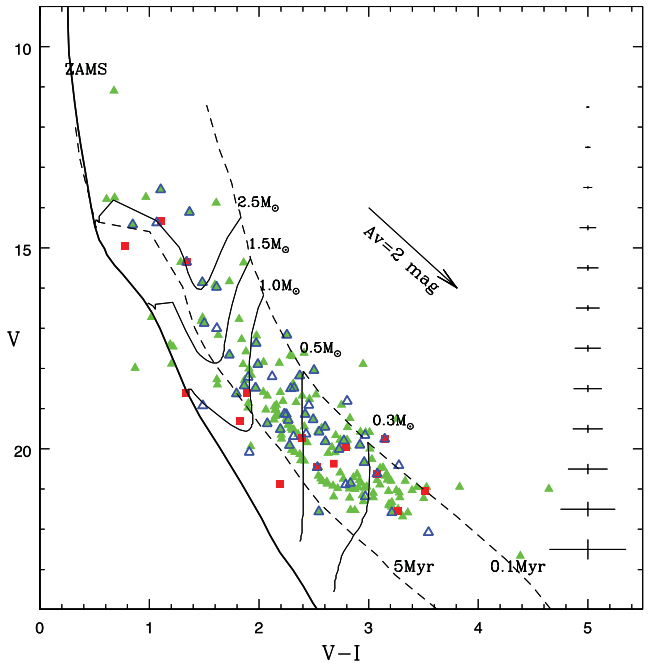

Figure 8. $V/(V-I)$ CMD for the identified candidate YSOs in Sh2-252 within the area shown by solid lines in Fig. 1. The Class I and Class II sources are shown with red squares and green filled triangles, respectively, and the blue open triangles are the Hα emission-line sources. The thick solid curve is the locus of ZAMS from Girardi et al. (2002), dashed curves are the PMS isochrones of age 0.1 and 5 Myr, respectively, and the thin solid curves are the evolutionary tracks for various mass bins from Siess et al. (2000). All the isochrones and tracks are corrected for the distance and reddening. The arrow indicates the reddening vector for $A_V = 2$ mag. The average error in $(V-I)$ colour as a function of magnitude is shown in the right-hand side of the figure.

track is given towards its right), which indicate that a majority of the YSOs have masses in the range between 0.3 and 2.5 $M_\odot$.

The ages of the young clusters/H II regions can also be derived from the post-main-sequence age of their most massive members. The most massive member of Sh2-252 is HD 42088, an O6.5 star which is still in the MS (Conti & Alschular 1971; Walborn 1972) and is considered to be the main ionizing source of Sh2-252. Also, none of the spectroscopically identified OB stars of Sh2-252 is found to be evolved (see section 3.1). Hence, the age of the H II region Sh2-252 should be younger or of the order of the MS lifetime of the O6.5V star. i.e. ∼4.4 Myr (Meynet et al. 1994). Thus, we can put an upper limit to the age of Sh2-252 as ∼4 Myr. However, this has to be taken as an approximate estimate as the low-mass members of the region could have been formed prior to HD 42088.

3.4 Stellar contents of the sub-regions in Sh2-252

3.4.1 Ionizing sources of the CH II regions

As discussed in Section 1.1, the radio observation of this region by Felli et al. (1977) identified six compact thermal radio sources, of which the regions A, B, C and E have been claimed as CH II regions having its own ionizing sources in each of them. In order to search for the ionizing sources of these regions, we obtained spectra of optically bright sources within 2 arcmin radius around each region. The spectral types of these bright sources have been discussed in Section 3.1 and each region is found to have at least one source with spectral type earlier than B3V. Their spectral type can also be obtained by measuring the number of Lyman continuum photons ($N_{\rm lyc}$) emitted per second by the star that would be responsible for the ionization of each region. From the radio continuum flux at 1415 MHz by Felli et al. (1977) together with our estimated distance of 2.4 kpc and assuming an electron temperature of 10^4 K, we calculated log $N_{\rm lyc}$ using the relation given by Martín-Hernández, van der Hulst & Tielens (2003). The log $N_{\rm lyc}$ have been obtained as 46.73, 47.52, 46.57 and 46.55, respectively, for regions A, B, C and E. From these log $N_{\rm lyc}$ values we derived the spectral type of the ionizing sources (Panagia 1973) as B0-B0.5, B0, B0.5 and B0.5, respectively, for regions A, B, C and E. These spectral types are consistent with the earliest spectral types derived by our optical observations for regions A, B and E (i.e. stars 3, 11 and 5; see Table 4) within the errors. The 1280 MHz observations by Tej et al. (2006) also estimated the spectral type of the ionizing source of region A as B0-B0.5V, which is consistent with our estimate. Slight difference in the spectral-type estimate is expected due to uncertainties in the effective temperature and ionizing flux of massive stars, for a given spectral type. Thus we conclude that the stars 3, 11 and 5 are the ionizing sources of the CH II regions A, B and E, respectively. However in the present observation, the earliest spectral type derived in region C is B2.5V (see Table 4), which does not seem to be early enough to explain the radio continuum flux. The expected spectral type from the radio flux is much earlier than B2.5V. The study by Kömpe et al. (1989) showed that the probable spectral type of the *IRAS* point source (IRAS 06063+2040) located at the centre of the nebulosity in region C is B0V, which could be the candidate ionizing source of this CH II region. Since this source is deeply embedded in the cloud ($K = 9.16$, $A_V \sim 8$ mag), we could not carry out optical spectroscopy of this source, and future spectroscopy would help us to confirm this result. In Fig. 9 we have shown the K_S-band images of the sub-regions A, B, C, E, NGC 2175s and Teu 136 for an area 8×8 arcmin^2. The probable ionizing sources of the regions A, B, C and E are marked with a white star symbol.

3.4.2 Stellar surface density distribution in Sh2-252

Although we have the optical and NIR observations for an area $\sim 1 \times 1$ deg^2 around the Sh2-252 region, majority of the members of Sh2-252 might be confined within its sub-regions (see section 1.1). In order to define the extent of each sub-region and to study the morphology of the region, we generated isodensity contours for stellar population detected in 2MASS K band. The two-dimensional stellar surface density distribution of the Sh2-252 region manifests prominent stellar density enhancements at the locations of A, C, E, NGC 2175s and Teu 136. This indicates the presence of clustering associated with these sub-regions. On the other hand, no clustering is apparent towards the sub-regions B and F. In Fig. 9 the stellar surface density contours above 3σ of the background level are overplotted on the K_S-band images of regions A, B (no contours although), C, E, NGC 2175s and Teu 136. We will discuss the properties of these five sub-regions, i.e. A, C, E, NGC 2175s and Teu 136, individually in the ensuing sections. The extent of these sub-regions is estimated on the basis of the surface density distribution. The contour above the 3σ background level around each region is considered as its extent. Thus we estimated the radius as 3.5, 3.5, 3.0, 3.0, 3.0 arcsec, respectively, for the regions A, C, E, NGC 2175s and Teu 136. We used these extents for further analysis of these sub-regions.

3.4.3 NIR colour–colour diagrams

NIR CC diagrams are ideal tools to identify the candidate PMS sources having NIR excess (Hunter et al. 1995; Haisch, Lada &

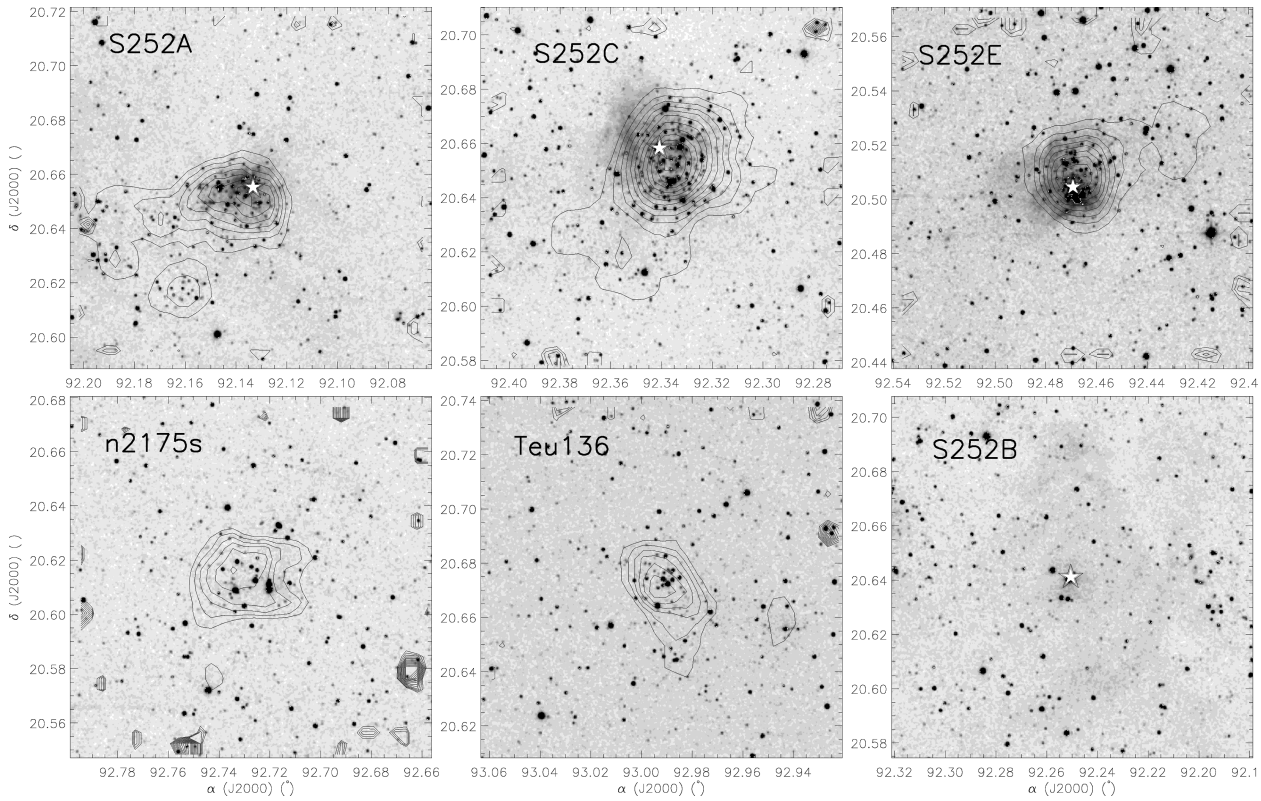

Figure 9. 8×8 arcmin^2 K_S-band images of the sub-regions within Sh2-252. The contours are the stellar surface density distribution generated by using all the sources detected in the K_S band. The ionizing sources of the CH II regions are also marked using the white star symbol.

Lada 2000, 2001; Sugitani et al. 2002; Devine et al. 2008; Chavarria et al. 2010). The $(J-H)/(H-K)$ CC diagrams for the sub-regions A, C, E, NGC 2175s and Teu 136 and a nearby control field are shown in Fig. 10. We have considered an area of 3.0 arcsec radius centred at $\alpha_{2000} = 06^{\rm h}09^{\rm m}30^{\rm s}$, $\delta_{2000} = +20^{\circ}08'$ as the control field. This region is devoid of nebulosity in the R band (see Fig. 1), and hence can be considered as a field region. The thin and thick solid curves are the locations of unreddened MS and giant stars (Bessell & Brett 1988), respectively. The dotted lines represent the locus of intrinsic and reddened ($A_V = 4.0$ mag; 8.0 mag) classical T Tauri stars (CTTSs; Meyer et al. 1997). The two long parallel dashed lines are the reddening vectors for the early MS and giant-type stars (drawn from the base and tip of the two branches). One more reddening vector is plotted from the tip of the unreddened CTTS locus. The crosses on the reddening vectors are separated by an A_V value of 5 mag. The extinction ratios, $A_J/A_V = 0.265, A_H/A_V = 0.155$ and $A_K/A_V = 0.090$, are adopted from Cohen et al. (1981). The magnitudes, colours of the stars and the curves are in the CIT system.

Following Ojha et al. (2004a), we classified sources according to their locations in $(J-H)/(H-K)$ CC diagrams. The 'F' sources are those located between the reddening vectors projected from the intrinsic colours of MS and giant stars. These sources are reddened field stars (MS and giants) or Class III/Class II sources with little or no NIR excess [viz. weak-lined T Tauri sources (WTTSs) but some CTTSs may also be included]. The sources located redwards of region 'F' are considered to have NIR excess. Among these, the 'T' sources are located redwards of 'F' but bluewards of the reddening line projected from the red end of the CTTS locus. These sources are considered to be mostly CTTSs (Class II objects) with large NIR excesses (Lada & Adams 1992). There may be an overlap in NIR colours of Herbig Ae/Be stars and T Tauri stars in the 'T' region (Hillenbrand et al. 1992). The 'P' sources are those located in the region redwards of region 'T' and are most likely Class I objects (protostellar-like) showing large amount of NIR excess. Here it is worthwhile to mention that Robitaille et al. (2006) have shown that there is a significant overlap between protostellar-like objects and CTTSs in the CC diagram.

A comparison of the distribution of sources in the sub-regions and the control field in Fig. 10 suggests that there is an appreciable difference between them. A significant fraction of sources within the sub-regions are concentrated between the intrinsic and reddened CTTS locus (i.e. within the 'F' and 'T' regions), whereas a majority of the sources in the control field are mainly concentrated towards the left of the 'F' region [i.e. $(H-K) < 0.35$ mag]. Average value of the uncertainty in $(H-K)$ colour is $\sim$0.05 mag. Taking this uncertainty into consideration and on the basis of the comparison of the CC diagrams, we can safely assume that a majority of the sources in the sub-regions located between the intrinsic and reddened CTTS locus with $(H-K) > 0.40$ mag and lying in the 'F', 'T' and 'P' regions are most likely PMS members. Some of the above sources lying in the 'F' region could be the reddened field stars; however a majority of them are likely candidate WTTSs or CTTSs with little or no NIR excess. Fig. 10 shows that the clusters NGC 2175s and Teu 136 do not have many PMS members with $A_V > 4.0$ mag, whereas a significant fraction of the PMS members of the sub-regions A, C and E are reddened up to 8.0 mag. This indicates that the clusters NGC 2175s and Teu 136, which are located towards the east of Sh2-252, are less reddened in comparison to other sub-regions of Sh2-252 located towards the west.

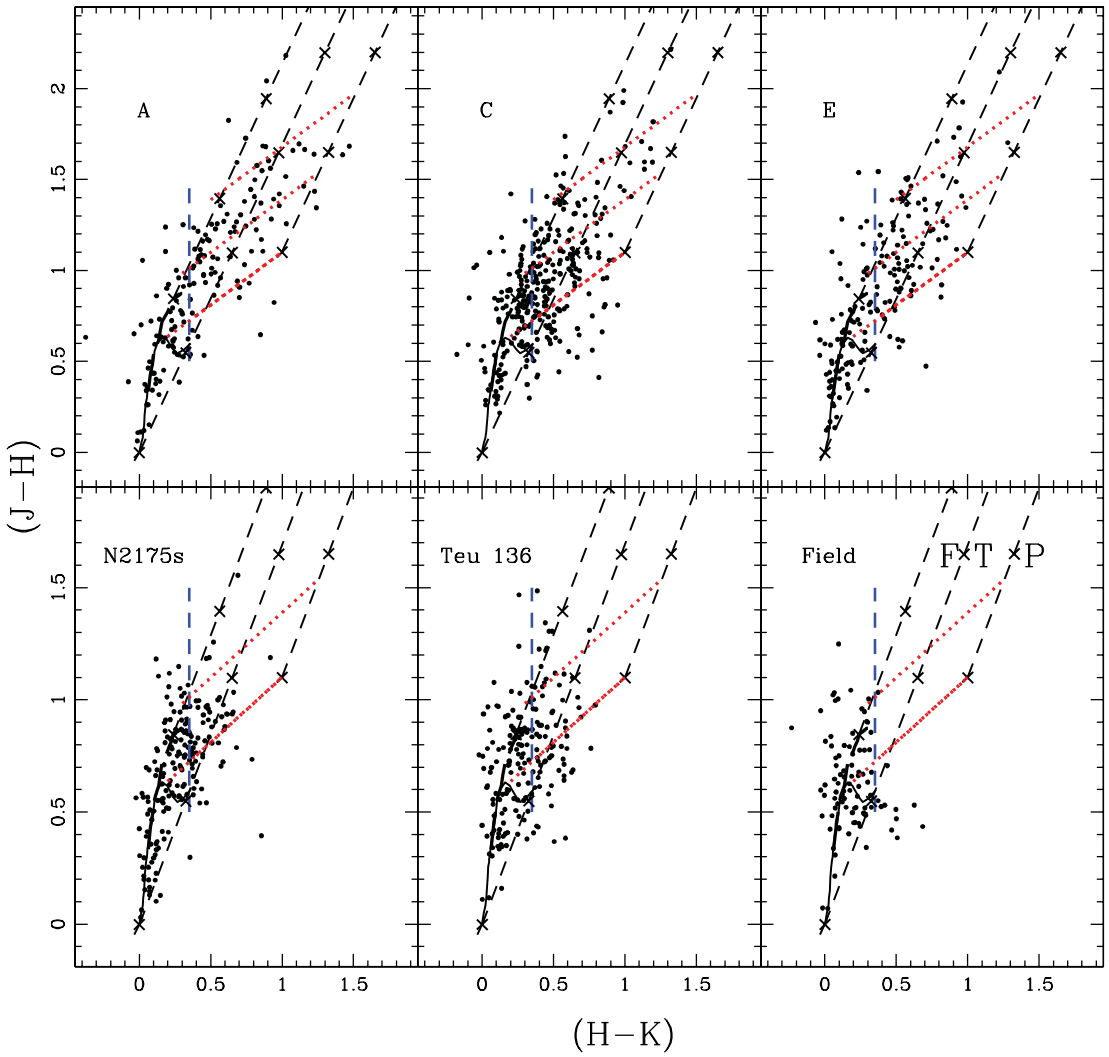

Figure 10. $(J-H)/(H-K)$ CC diagrams of the sources detected in the *JHK* bands within the sub-regions of Sh2-252 and a nearby control field. The regions are marked in the figure. The locus for dwarfs (the thin solid curve) and giants (the thick solid curve) are from Bessell & Brett (1988). The red dotted lines represent the intrinsic and reddened ($A_V = 4.0$ mag; 8.0 mag) locus of CTTSs (Meyer et al. 1997). The dashed lines in black represent the reddening vectors (Cohen et al. 1981). The crosses on the dashed lines are separated by $A_V = 5$ mag. The blue vertical line divides the $(H-K)$ colour at 0.35 mag (see the text).

3.4.4 Optical colour–magnitude diagrams

The $V/(V-I)$ CMDs for the sources within the sub-regions of Sh2-252 and the nearby control field are shown in Fig. 11. The ZAMS (thick solid curve) by Girardi et al. (2002) and PMS isochrones (dashed curves) by Siess et al. (2000) for age 0.1 and 5 Myr are also shown. The ZAMS and isochrones are shifted for the distance of 2.4 kpc and reddening of $A_v = 0.5$ mag. The encircled sources are those located above the intrinsic CTTS locus in the $(J-H)/(H-K)$ CC diagram (Fig. 10) and with $(H-K) > 0.4$ mag. A majority of these sources are found to have ages <5 Myr in all the sub-regions, suggesting that the sources with $(H-K) > 0.4$ mag could be probable PMS members as discussed in Section 3.4.3. A comparison of these CMDs with that of the control field also supports the notion that the sources lying between 0.1 and 5 Myr isochrones could be the PMS sources associated with the sub-regions. Similarly, the CMDs of the sub-regions resemble the $V/(V-I)$ CMD for the candidate YSOs shown in Fig. 8. It further supports that the majority of the sources identified on the basis of $(J-H)/(H-K)$ CC diagrams (Fig. 10) in the sub-regions could be the PMS members and that they have an age spread of 5 Myr. A detailed analysis on the evolutionary status of the YSOs within the individual regions will be done in a forthcoming paper.

3.5 *K*-band luminosity functions of sub-regions in Sh2-252

The LF in the *K* band is frequently used in studies of young clusters and SFRs as a diagnostic tool of the MF and the star formation history of their stellar populations. Pioneering work on the interpretation of KLF was presented by Zinnecker, McCaughrean & Wilking (1993). During the last decade several studies have been carried out with the aim of determining the KLF of young clusters (e.g. Muench, Lada & Lada 2000; Lada & Lada 2003; Ojha et al. 2004b; Sanchawala et al. 2007; Pandey et al. 2008; Jose et al. 2008, 2011). We used the 2MASS *K*-band data to study the KLF of the Sh2-252 region. Because this region shows clusterings around the regions A, C, E, NGC 2175s and Teu 136 (see Section 3.4.2), we estimated the KLF for each region independently. The KLF is calculated within the area of each region as estimated on the basis of stellar surface density distribution discussed in Section 3.4.2.

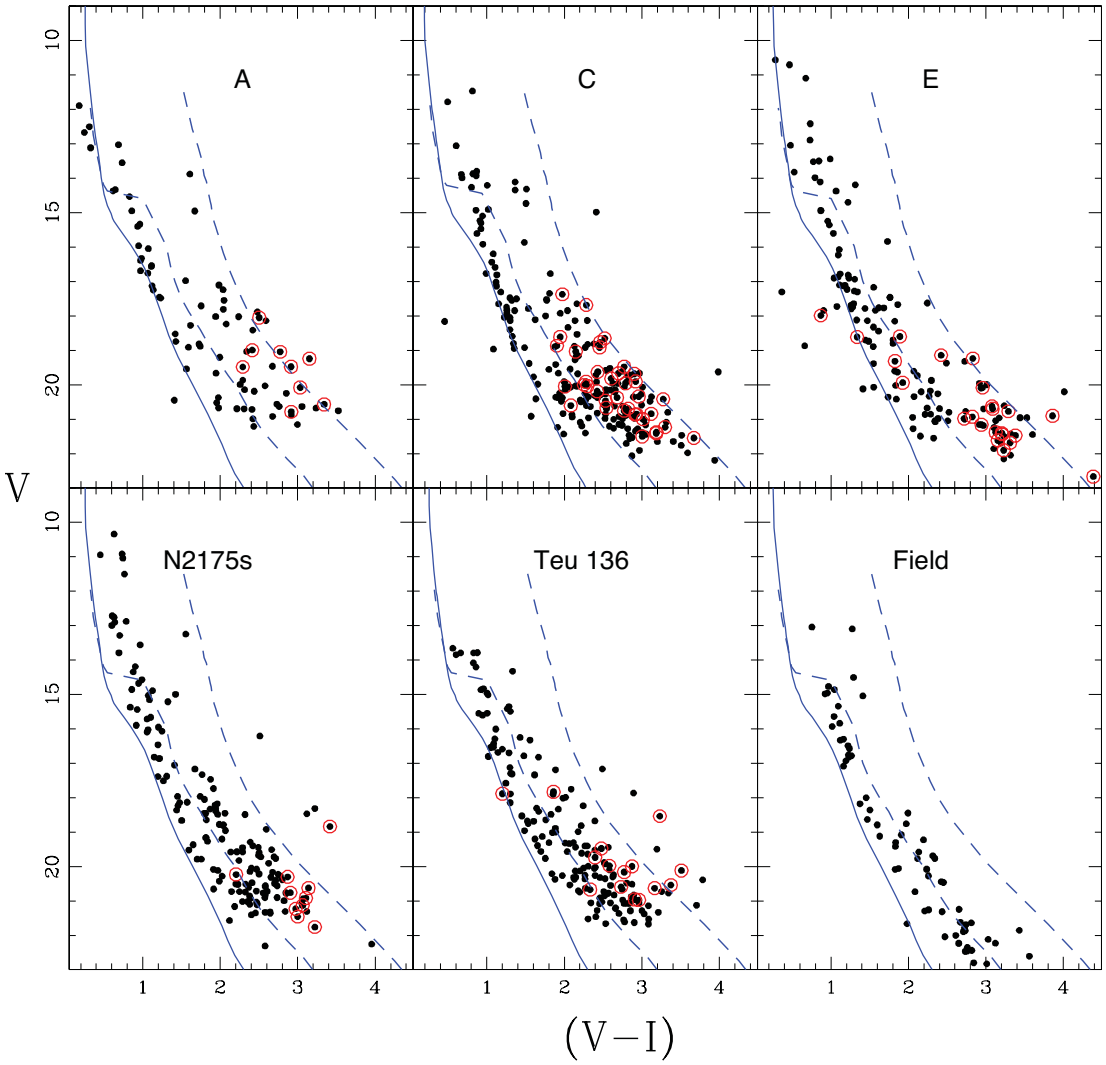

Figure 11. $V/(V-I)$ CMDs for the sources within the sub-regions of Sh2-252 and the nearby control field. The sub-regions are marked in the figure. Encircled are the sources with $(H-K) > 0.4$ mag and are located above the intrinsic CTTS locus of the $(J-H)/(H-K)$ CC diagram (Fig. 10). The thick solid curve is the ZAMS from Girardi et al. (2002) and the dashed curves are the PMS isochrones of age 0.1 and 5 Myr, respectively, from Siess et al. (2000), corrected for the distance and reddening.

KLF is the number of stars as a function of K-band magnitude. In order to convert the observed KLF to the true KLF, it is necessary to account for the data incompleteness as well as the background and foreground source contamination. The regions C and NGC 2175s were corrected for their respective CFs given in Table 3 and the average value of the CFs for regions C and NGC 2175s was applied to regions A, E and Teu 136 to correct for their data incompleteness. The data from the control field region (see Section 3.4.3) have been used to remove the field star contribution. Since this control field is located off the Sh2-252 region, its background population will be affected by a smaller interstellar reddening, whereas the background field stars of the sub-regions of Sh2-252 are seen through a larger reddening due to the matter associated with it. Hence the population in the background of sub-regions will be more reddened as compared to the control field. Therefore a direct subtraction of the observed control field from the sub-regions of Sh2-252 will yield incorrect LF. To account for the higher extinction towards the embedded sub-regions, the field star population towards the direction of the control field is predicted on the basis of the Besançon Galactic model of stellar population synthesis (Robin et al. 2003) by using a similar procedure as described by Ojha et al. (2004b). An advantage of using this model is that we can simulate foreground ($d < 2.4$ kpc) and the background ($d > 2.4$ kpc) field star populations separately. The foreground population was simulated by using the model with the extinction $A_V = 1.1$ mag [$E(B-V) = 0.35$ mag; cf. section 3.2] and $d < 2.4$ kpc. As discussed in Section 3.4.3, a majority of the PMS members of regions A, C and E are reddened up to $A_V = 8.0$ mag, whereas in NGC 2175s and Teu 136 they are reddened up to $A_V = 4.0$ mag. Hence the background population in these regions are seen through clouds with extinction of 8.0 and 4.0 mag, respectively. Hence, we simulated two sets of background population ($d > 2.4$ kpc) with A_V values of 4.0 and 8.0 mag, respectively. Then we determined the fractions of the contaminating stars (foreground + background) over the total model counts. The fraction was calculated separately for both sets of the simulated background population. These fractions were used to scale the nearby observed control field and subsequently the star counts of the modified control field were subtracted from the KLFs of the sub-regions of Sh2-252 to obtain their final corrected KLFs.

The KLFs of young embedded clusters are known to follow power-law shapes (Lada et al. 1991; Lada, Young & Greene 1993), which is expressed as

$$\frac{dN(K)}{dK} \propto 10^{\alpha K}$$

where $\frac{dN(K)}{dK}$ is the number of stars per 1 mag bin and α is the slope of the power law. We counted the number of stars per unit magnitude interval after correcting for the field star contribution. We then fit a power law to the data. The resulting field star subtracted KLFs for the five sub-regions of Sh2-252 are shown in Fig. 12. The slopes of the KLFs of regions A, C, E, NGC 2175s and Teu 136 have been obtained as 0.31 ± 0.03, 0.34 ± 0.03, 0.25 ± 0.05, 0.20 ± 0.05 and 0.36 ± 0.02, respectively. Within errors, the KLFs for all the five regions seem to match with each other.

KLFs of clusters of different ages are known to have different peak magnitudes and slopes (Muench et al. 2000) and hence the KLF slope could be an age indicator of young clusters. For clusters up to 10 Myr old, the KLF slope gets steeper as the cluster gets older (Ali & Depoy 1995; Lada & Lada 1995). However, there exists no precise age–KLF relationship in the literature due to huge uncertainties in their correlation (Devine et al. 2008). There are many studies on KLF of young clusters. The studies by Blum, Conti & Damineli (2000), Figuerêdo et al. (2002), Leistra et al. (2005), Leistra, Cotera & Liebert (2006) and Devine at al. (2008) indicate that the KLF slope varies from 0.2 to 0.4 for clusters younger than 5 Myr, which is in agreement with the KLFs obtained for the sub-regions of Sh2-252. The KLFs of the sub-regions of Sh2-252 are worth comparing with the recent studies of SFRs viz. NGC 1893 (Sharma et al. 2007), Be 59 (Pandey et al. 2008), Stock 8 and NGC 1624 (Jose et al. 2008, 2011), since all the KLFs are obtained by using a similar technique. The slopes of the KLFs obtained for the sub-regions in Sh2-252 are comparable with those obtained for NGC 1893 ($\alpha = 0.34 \pm 0.07$), Stock 8 ($\alpha = 0.31 \pm 0.02$), Be 59 ($\alpha = 0.27 \pm 0.02$) and NGC 1624 ($\alpha = 0.30 \pm 0.06$).

3.6 Initial mass functions of sub-regions in Sh2-252

One of the most fundamental disciplines of astrophysical research is the origin of stars and stellar masses. The distribution of stellar masses that form in a star formation event in a given volume of space is called IMF and is one of the most important measurable quantities in star formation studies. Together with star formation rate, the IMF dictates the evolution and fate of star clusters and

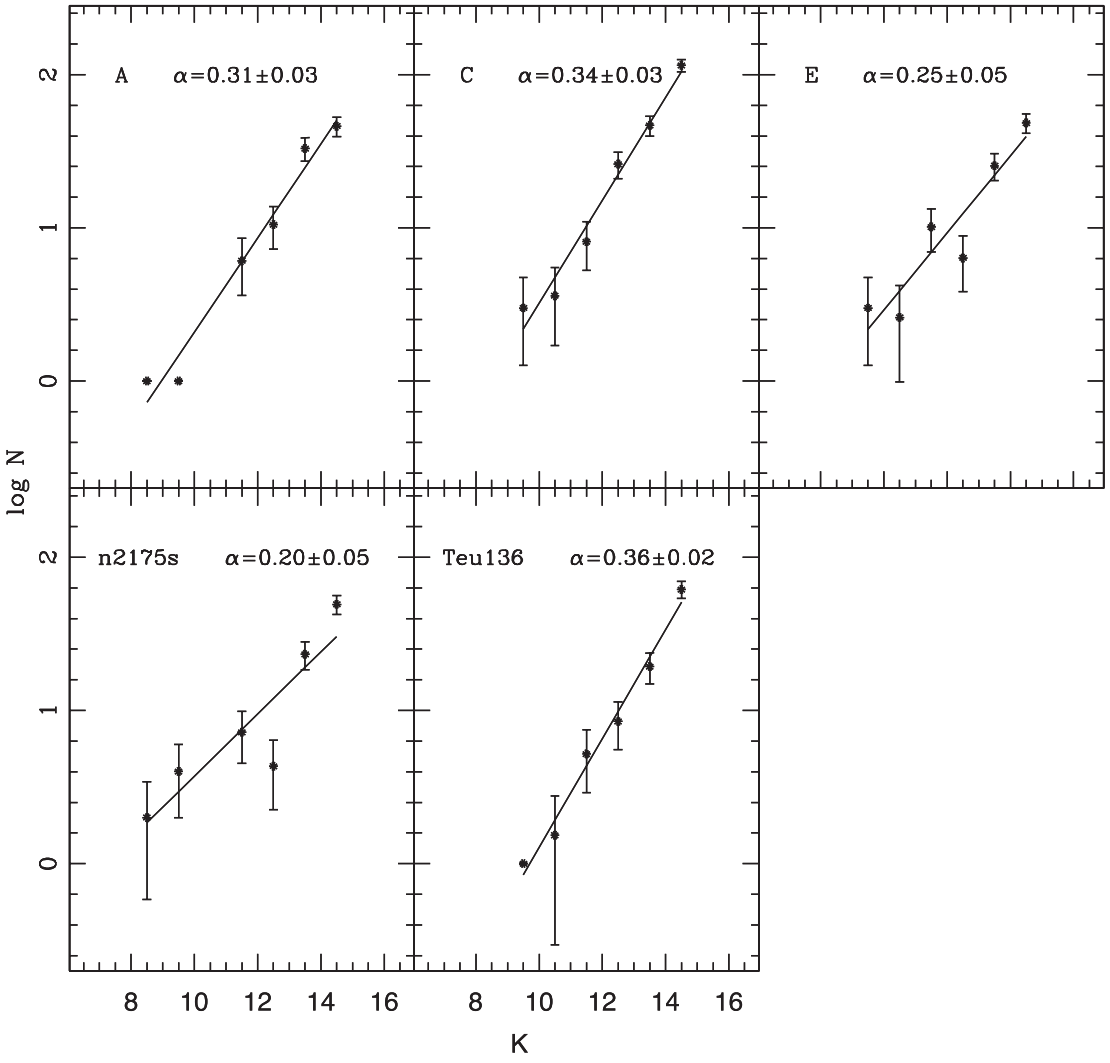

Figure 12. KLFs derived for the sub-regions in Sh2-252 after subtracting the field star contamination (see the text). The error bars represent the $\pm \sqrt{N}$ errors. The linear fits are represented by the straight lines and the slopes obtained are given in each figure.

galaxies (Kroupa 2002). Young clusters and SFRs are important objects to study the IMF since their MFs can be considered as IMFs as they are too young to lose a significant number of members by either dynamical or stellar evolution.

The MF is often expressed by the power law, $N(\log m) \propto m^{\Gamma}$ and the slope of the MF is given as

$$\Gamma = \mathrm{d}\log N(\log m)/\mathrm{d}\log m,$$

where $N(\log m)$ is the number of stars per unit logarithmic mass interval. For the mass range $0.4 < \mathrm{M/M_{\odot}} \leq 10$, the classical value derived by Salpeter (1955) is $\Gamma = -1.35$.

One of the main objectives of this work is to measure the MFs of the sub-regions of Sh2-252. As discussed in Section 3.4.4, the majority of the sources lying above the 5 Myr isochrone of the CMDs could be probable PMS members of the region and most of them have a mass range of 0.3–2.5$\mathrm{M_{\odot}}$. We calculated the MFs of these PMS sources falling above 5 Myr and mass range of 0.3–2.5 $\mathrm{M_{\odot}}$ for the five sub-regions. To remove the contamination due to field stars from the PMS sample, we statistically subtracted the contribution of field stars from the observed CMDs of sub-regions (see Fig. 11) using the procedure described in our earlier studies (e.g. Jose et al. 2008, 2011; Pandey et al. 2008). After statistically subtracting the field star contribution, we used all the candidate PMS sources lying above the 5 Myr isochrone and having mass in the range of 0.3–2.5 $\mathrm{M_{\odot}}$ to calculate the MFs. The MFs for the candidate PMS sources were obtained by counting the number of stars in various mass bins, shown as evolutionary tracks by Siess et al. (2000) in Fig. 8. Necessary corrections for data incompleteness as a function of magnitude were taken into account to calculate the MFs. The CFs given in Table 3 for regions C and NGC 2175s were used to correct for their data incompleteness whereas the average value of the CFs for regions C and NGC 2175s was applied to regions A, E and Teu 136 to correct for their data incompleteness. The resulting field star decontaminated and completeness corrected MFs of the PMS sources of the five sub-regions of Sh2-252 region are shown in Fig. 13. The slopes, Γ, of the MFs in the mass range $0.3 \leq \mathrm{M/M_{\odot}} < 2.5$ are found to be -1.33 ± 0.51, -2.39 ± 0.15, -1.40 ± 0.30, -1.65 ± 0.28, -1.82 ± 0.26, respectively, for regions A, C, E, NGC 2175s and Teu 136. The slopes of the MFs of the regions A and E are in good agreement with that of

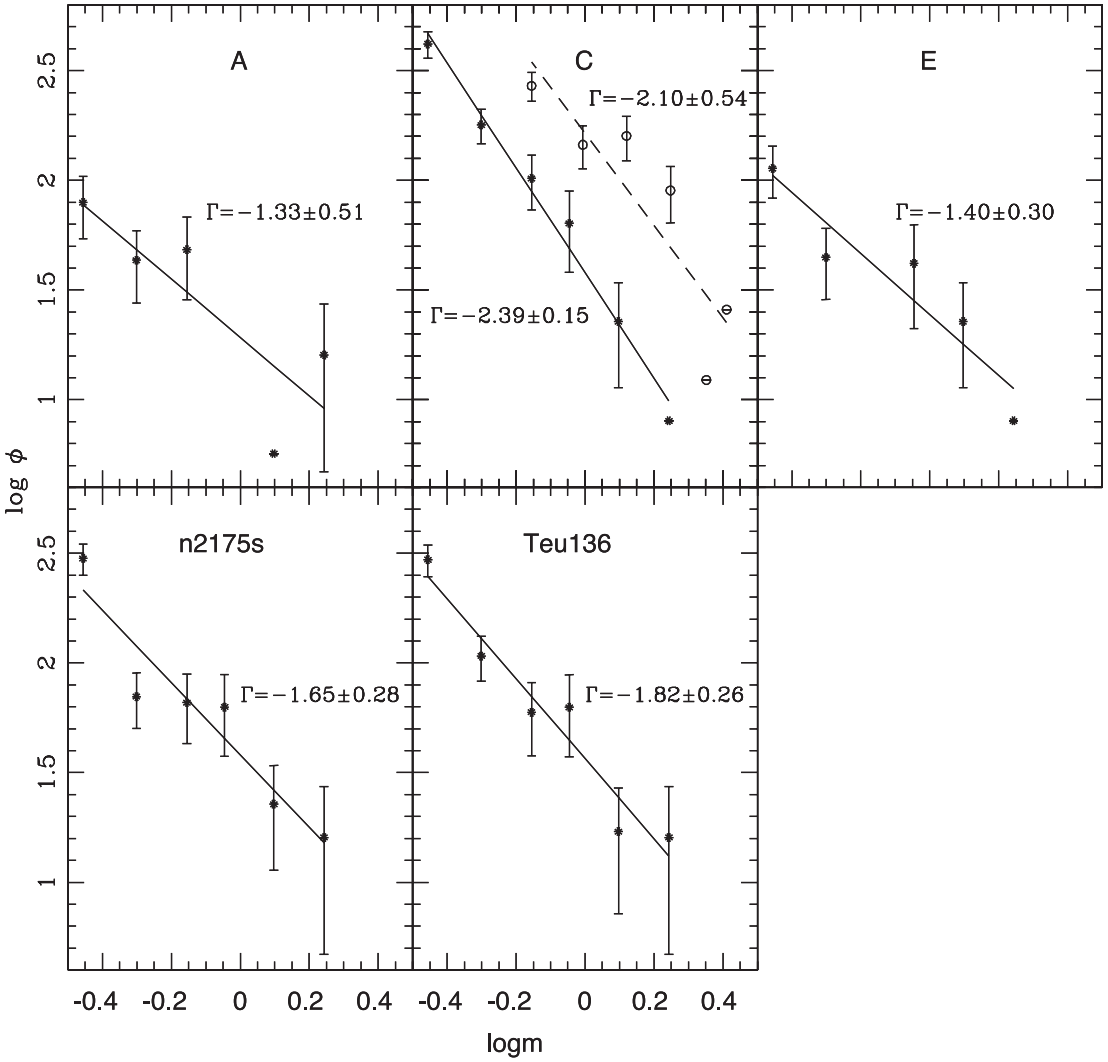

Figure 13. MFs obtained from the optical data for the sub-regions of Sh2-252 after correcting for the field star contamination and data incompleteness. The ϕ represents N/dlog m and the error bars represent $\pm\sqrt{N}$ errors. The continuous lines show least-squares fits to the mass ranges described in the text. The value of the slopes obtained are given in each figure. The MF obtained from JLF for region C is shown in the second panel and the least-squares fit is shown by using the dashed line.

the Salpeter (1955) value, and in view of large errors, those in the case of NGC 2175s and Teu 136 can also be considered comparable to the Salpeter value. However, in the case of the region C, the MF seems to be steeper than the Salpeter value. In order to check this we also calculated the MF using *J*-band luminosity function (JLF). The procedure for this calculation has been mentioned in our earlier paper (Jose et al. 2011). The MF thus obtained for region C from JLF is shown in Fig. 13 as the dashed line and the slope obtained is -2.10 ± 0.54. Considering the large uncertainty in the IMF calculation, we conclude that all the regions have IMF slopes, which do not significantly deviate from the Salpeter value.

The shape of the stellar IMF and whether it is universal or not are key issues in astrophysics. For clusters within 2 kpc, there is no compelling evidence for variations in the stellar IMF with respect to their environment (e.g. Meyer et al. 2000; Kroupa 2002; Chabrier 2005). We have been pursuing studies of various SFRs in the Galaxy, hence a comparative study of their IMFs obtained using similar techniques will give useful information on IMFs. Our recent analyses of young clusters (age 2–4 Myr), viz. NGC 1893 (Sharma et al. 2007), Stock 8, NGC 1624 (Jose et al. 2008, 2011) and W5 E (Chauhan et al. 2011), has yielded values similar to the Salpeter value. In the present study, the MFs of all the sub-regions of Sh2-252 are found to be in general comparable to the Salpeter value.

4 SUMMARY

In this paper we studied the stellar contents of the H II region Sh2-252 which itself contains four CH II regions, A, B, C and E, and two clusters, NGC 2175s and Teu 136. We used the deep optical photometry in *UBVRI* bands, slit and slitless spectroscopic observations along with the *JHK* data from 2MASS for our analyses. An attempt has been made to identify and classify the massive members to determine the fundamental parameters of Sh2-252 as well as to obtain the age and mass distribution of candidate PMS sources and finally to constrain the KLFs and IMFs of the sub-regions of Sh2-252.

We have carried out optical spectroscopy of 15 bright sources of the region, out of which eight have been identified as massive members of spectral type earlier than B3. The CH II regions A, B, C and E are found to have at least one star of spectral type earlier than B3, whereas the small optically bright cluster NGC 2175s is found to have four stars of spectral type earlier than B3 around its centre. We have also identified the probable candidate ionizing sources of the CH II regions A, B, C and E. From the spectrophotometric analyses, we derived the average distance of the region as 2.4 ± 0.2 kpc. The distance estimated from the four bright stars of NGC 2175s is found to be in good agreement with the average distance of Sh2-252, which supports the association of NGC 2175s with the Sh2-252 complex. In this paper, we also report that the NIR embedded cluster Teu 136, located at the eastern edge of the complex as a sub-cluster of Sh2-252. Based on the optical CC diagram and spectroscopic properties, the reddening $E(B-V)$ of the massive members of the region is found to vary between 0.35 to 2.1 mag.

Using slitless spectroscopy survey, we have identified 61 Hα emission sources in the region. We obtained optical photometry for 211 candidate YSOs of the region. The distribution of these candidate YSOs on the $V/(V-I)$ CMD shows that a majority of them have an age distribution between 0.1 and 5 Myr and masses in the range of 0.3–2.5 $M_{\odot}$. The stellar surface density distribution in *K* band shows that there is at least five sub-clusters, each associated with the regions A, C, E, NGC 2175s and Teu 136. The $(J-H)/(H-K)$ CC diagrams of the individual regions show that the regions A, C and E have more reddened population when compared to the clusters NGC 2175s and Teu 136, which are located towards the east of Sh2-252. The optical CMDs of the individual regions also show that the candidate PMS sources are distributed between 0.1 and 5 Myr, suggesting an age spread for them.

We also calculated the KLFs of the sub-regions A, C, E, NGC 2175s and Teu 136 and have estimated as 0.31 ± 0.03, 0.34 ± 0.03, 0.25 ± 0.05, 0.20 ± 0.05 and 0.36 ± 0.02, respectively. Within errors, the KLFs of all the sub-regions are similar and comparable to that of young clusters of age < 5 Myr. We also derived the MFs of the PMS sample of the individual regions in the mass range of 0.3–2.5 $M_{\odot}$. The slopes of the MFs of all the sub-regions are found to match with the Salpeter value.

ACKNOWLEDGMENTS

The authors thank the anonymous referee for the useful comments, which improved the content and presentation of the paper significantly. We also thank the staff of the Kiso Observatory, Japan, ARIES, Naini Tal, India and IAO, Hanle, and its remote control station at CREST, Hosakote, for their assistance during the observations. This publication also makes use of data from the 2MASS, which is a joint project of the University of Massachusetts and the Infrared Processing and Analysis Center/CIT, funded by the National Aeronautics and Space Administration and the National Science Foundation. JJ and NC are grateful for the financial support for this study through a stipend from CSIR and DST, India. AKP is grateful to DST (India) and JSPS (Japan) for providing funds to visit Kiso observatory to carry out the observations.

REFERENCES

Ali B., Depoy D. L., 1995, AJ, 109, 709
Bessell M., Brett J. M., 1988, PASP, 100, 1134
Blum R. D., Conti P. S., Damineli A., 2000, AJ, 119, 1860
Bonatto C., Bica E., 2011, MNRAS, 414, 3769
Carpenter J. M., 2001, AJ, 121, 2851
Carraro G., Vazquez R. A., Moitinho A., Baume G., 2005, ApJ, 630, L153
Chabrier G., 2005, The Initial Mass Function 50 Years Later, Vol. 327, p. 41
Chauhan N., Pandey A. K., Ogura K., Jose J., Ojha D. K., Samal M. R., Mito H., 2011, MNRAS, 415, 1202
Chavarría K. C., de Lara E., Hasse I., 1987, A&A, 171, 216
Chavarría K. C., Leitherer C., de Lara E., Sanchez O., Zickgraf F.-J., 1989, A&A, 215, 51
Chavarria L., Mardones D., Garay G., Escala A., Bronfman L., Lizano S., 2010, ApJ, 710, 583
Churchwell E., 1974, in Proc. Second European Regional Meeting in Astron. Mem. Soc. Astron. Ital. Vol. 45, p. 259
Clarke C. J., 2007, MNRAS, 376, 1350
Cohen J. G., Frogel J. A., Persson S. E., Ellias J. H., 1981, ApJ, 249, 481
Conti P. S., Alschular W. R., 1971, ApJ, 170, 325
Cutri R. M. et al., 2003, The IRSA 2MASS All Sky Point Source Catalog, NASA/IPAC Infrared Science Archive, http://irsa.ipac.caltech.edu/applications/Gator/
Dahm S., 2005, AJ, 130, 1805
Devine K. E., Churchwell E. B., Indebetouw R., Watson C., Crawford S. M., 2008, AJ, 135, 2095
Elmegreen B. G., Lada C. J., 1977, ApJ, 214, 725
Felli M., Habing H. J., Israël F. P., 1977, A&A, 59, 43
Figuerêdo E., Blum R. D., Damineli A., Conti P. S., 2002, AJ, 124, 2739
Garnier R., Lortet-Zuckermann M. C., 1971, A&A, 31, 41
Georgelin Y. P., Georgelin Y. M., 1970, A&A, 6, 349

Girardi L., Bertelli G., Bressan A., Chiosi C., Groenewegen M. A. T., Marigo P., Salasnich B., Weiss A., 2002, A&A, 391, 195
Grasdalen G. L., Carrasco L., 1975, A&A, 43, 259
Gutermuth R. A., Megeath S. T., Myers P. C., Allen L. E., Pipher J. L., Fazio G. G., 2009, ApJS, 184, 18
Haikala L. K., 1994, A&A, 108, 643
Haisch K. E., Lada E. A., Lada C. J., 2000, AJ, 120, 1396
Haisch K. E., Lada E. A., Lada C. J., 2001, AJ, 121, 2065
Hernandez J., Calvet N., Hartmann L., Briceno C., Sicilia-Aguilar A., Berlind P., 2005, AJ, 129, 856
Hillenbrand L. A., Strom S. E., Vrba F. J., Keene J., 1992, ApJ, 397, 613
Hunter T. R., Testi L., Taylor G. B., Tofani G., Felli M., Phillips T. G., 1995, A&A, 302, 249
Jacoby G. H., Hunter D. A., Christian C. A., 1984, ApJS, 56, 257
Jose J. et al., 2008, MNRAS, 384, 1675
Jose J. et al., 2011, MNRAS, 411, 2530
Kömpe C., Joncas G., Baudry A., Wouterloot J. G. A., 1989, A&A, 221, 295
Koornneef J., 1983, A&A, 128, 84
Koposov S. E., Glushkova E. V., Zolotukhin I. Yu., 2008, A&A, 486, 771
Kroupa P., 2002, Sci, 295, 82
Lada C. J., Adams F. C., 1992, ApJ, 393, 278
Lada E. A., Lada C. J., 1995, AJ, 109, 1682
Lada E. A., Evans N. J., Depoy D. L., Gatley I., 1991, ApJ, 371, 171
Lada C. J., Lada E. A., 2003, ARA&A, 41, 57
Lada C. J., Wooden D., 1979, ApJ, 232, 158
Lada C. J., Young T., Greene T., 1993, ApJ, 408, 471
Landolt A. U., 1992, AJ, 104, 340
Lee H. T., Chen W. P., Zhang Z. W., Hu J. Y., 2005, ApJ, 624, 808
Leistra A., Cotera A. S., Leibert J., Burton M., 2005, AJ, 130, 1719
Leistra A., Cotera A. S., Liebert J., 2006, AJ, 131, 2571
Martín-Hernández N. L., van der Hulst J. M., Tielens A. G. G. M., 2003, A&A, 407, 957
Meyer M., Calvet N., Hillenbrand L. A., 1997, AJ, 114, 288
Meyer M. R., Adams F. C., Hillenbrand L. A., Carpenter J. M., Larson R. B., 2000, Mannings V., Boss A. P., Russell S. S., eds, Protostars and Planets IV. Univ. Arizona Press, Tucson, p. 121
Meynet G., Maeder A., Schaller G., Schaerer D., Charbonnel C., 1994, A&AS, 103, 97
Muench A. A., Lada E. A., Lada C. J., 2000, ApJ, 553, 338
Neckel T., Klare G., Sarcander M., 1980, Bull. Inform. Centre, des Donees Stellaires, p. 19
Ojha D. K. et al., 2004a, ApJ, 608, 797
Ojha D. K. et al., 2004b, ApJ, 616, 1042
Panagia N., 1973, AJ, 78, 929
Pandey A. K., Nilakshi, Ogura K., Sagar R., Tarusawa K., 2001, A&A, 374, 504
Pandey A. K., Sharma S., Ogura K., 2006, MNRAS, 373, 255
Pandey A. K., Sharma S., Ogura K., Ojha D. K., Chen W. P., Bhatt B. C., Ghosh S. K., 2008, MNRAS, 383, 1241
Pismis P., 1970, Boletin Observatorio Tonantzintla Tacubaya, 5, 219
Pismis P., 1977, Rev. Mex. Astron. Astrofis., 2, 59
Reed B. C., 2003, AJ, 125, 2531
Reid M. J., Menten K. M., Brunthaler A., Zheng X. W., Moscadelli L., Xu Y., 2009, ApJ, 693, 397
Robin A. C., Reyle C., Derriere S., Picaud S., 2003, A&A, 409, 523
Robitaille T. P., Whitney B. A., Indebetouw R., Wood K., Denzmore P., 2006, ApJS, 167, 256
Salpeter E. E., 1955, ApJ, 121, 161
Sanchawala K. et al., 2007, ApJ, 667, 963
Schmidt-Kaler Th., 1982, in Schaifers K., Voigt H. H., Landolt H., eds, Landolt-Bornstein, Vol. 2b, Springer, Berlin, p. 19
Sharma S., Pandey A. K., Ojha D. K., Chen W. P., Ghosh S. K., Bhatt B. C., Maheswar G., Sagar R., 2007, MNRAS, 380, 1141
Sharpless S., 1959, ApJS, 4, 257
Siess L., Dufour E., Forestini M., 2000, A&A, 358, 593
Sugitani K. et al., 2002, ApJ, 565, L25
Szymczak M., Hrynek G., Kus A. J., 2000, A&AS, 143, 269
Tej A., ojha D. K., Ghosh S. K., Kulkarni V. K., Verma R. P., Vig S., Prabhu T. P., 2006, A&A, 452, 203
Torres-Dodgen A. V., Weaver W. B., 1993, PASP, 105, 693
Walborn N. R., 1972, AJ, 77, 312
Walborn N. R., Fitzpatrick E. L., 1990, PASP, 102, 379
Zinnecker H., McCaughrean M. J., Wilking B. A., 1993, in Levy E., Lunine J., eds, Protostars and Planets III. Univ. Arizona Press, Tucson, p. 429

This paper has been typeset from a TEX/LATEX file prepared by the author.